EXHUMATION OF THE SOUTHERN PYRENEAN FOLD-THRUST BELT FROM OROGENIC GROWTH TO DECAY

Caitlin Rushlow

A thesis submitted to the faculty of the University of North Carolina at Chapel Hill in partial fulfillment of the requirements for the degree of Master of Science in the Department of Geological Sciences.

Chapel Hill
2012

Approved by:

Dr. Jason Barnes

Dr. Drew Coleman

Dr. Kevin Stewart

ABSTRACT

CAITLIN RUSHLOW: EXHUMATION OF THE SOUTHERN PYRENEAN FOLD-THRUST BELT FROM OROGENIC GROWTH TO DECAY
(Under the direction of Dr. Jason Barnes)

We quantify the spatiotemporal patterns of exhumation across the southern fold-thrust belt (FTB) margin with apatite fission track (AFT) thermochronology and compare the results with existing deformation, exhumation, and sedimentation chronologies. Eighteen bedrock samples record exhumation ~90 to 10 Ma. Rocks from the range core (Axial Zone) record rapid exhumation that progresses east to west and north to south consistent with patterns of tectonically-driven uplift. Sediments shed into piggyback basins retain a detrital exhumation signal. Samples from other FTB structures record *in situ* exhumation, suggesting sedimentary burial of sufficient magnitudes to reset the AFT system. A major exhumation phase occurs at the boundary between the thick- and thin-skinned portions of the FTB wedge at 25-20 Ma. We suggest that this exhumation records uplift from sediment overloading the outboard FTB structures and/or wetter climate conditions. A final exhumation phase between ~20-10 Ma may be a response to base level lowering.

ACKNOWLEDGEMENTS

To all the people who helped and supported me through the course of my masters work, I am forever grateful. In particular I would like to acknowledge my advisor foremost, Dr. Jason Barnes; my parents, Mike and Terri Rushlow; my sister, Kristen Rushlow; and finally my friends George and Fiona Allen, Kyle Anderson, Iris Chen, Steven Clark, Drew Hill, Angela Kang, Mike McCann, Mandy Oberheu, Jingyuan Sun, Sara Thelen, and Ian Winkelstern, without whom this effort would not have been possible.

TABLE OF CONTENTS

LIST OF TABLES

Table

LIST OF FIGURES

Figure

I. INTRODUCTION

Tectonic and surfaces processes play important roles in the development of linked thrust belt-foreland basin systems. This is particularly true as they shift from active shortening to post-orogenic decay [*Allen*, 2008]. Critical wedge theory suggests that mountain belts accommodate shortening by developing a characteristic wedge-shaped form that prefers an equilibrium (critical) state defined by the mean topographic gradient and the basal decollement (taper) [*Chapple*, 1978]. Deformation, erosion, and sedimentation redistribute mass within the evolving wedge, influencing the topographic and structural expression of convergent tectonics [*Davis et al.*, 1983; *Dahlen et al*., 1984]. Numerical and analog models support critical wedge theory, demonstrating that the rates of surface processes affect crustal deformation from the scale of an entire range [*Beaumont et al.*, 1992; *Mugnier et al.*, 1997] to a single structure [*Storti and McClay*, 1995; *Simpson*, 2006; *Stockmal et al.*, 2007]. Therefore, quantifying the history of deformation, erosion, and sedimentation is important for understanding orogen evolution.

Continental collision zones develop bivergent deforming wedge geometries with dual foreland basins flanking a central range interior [e.g., *Argand*, 1916; *Suppe*, 1987; *Brandon and Vance*, 1992; *Muñoz*, 1992]. These mountain belts tend towards asymmetry across strike, forming a wider pro-wedge over the under-thrusting plate and a narrower retro-wedge over the overriding plate [*Willett et al.*, 1993; *Sinclair et al.*, 2005]. Orographic focusing of precipitation [*Willett*, 1999], oblique convergence [*Whitchurch et al.*, 2011], and crustal heterogeneities [*Beaumont et al.*, 2000] can perturb the deformation field and distribution of mass within an orogen, generating further asymmetry along and across strike. After orogenesis ceases, processes such as isostatic rebound [Gilchrist et al. 1994] and drainage basin reorganization [*Garcia-Castellanos et al.*, 2003] can continue to alter the orogenic system. Fold-thrust belts (FTBs) play major roles in how wedges accommodate shortening and adjust their state in response to changing perturbations [*Chapple*, 1978]. At the wedge margin, the common thin-skinned portion of the FTB occupies a key position that is characterized by localized uplift on thrust fault-driven hanging walls and deposition both within the wedge in piggyback basins and in the adjacent, flexure-driven subsiding foreland basin during active orogenesis [*DeCelles and Giles*, 1996]. Thus, FTB margins are ideal locations to investigate the interaction between surface processes and tectonics because they occupy the transition between hinterlands dominated by uplift and erosion and mountain belt margins, characterized by more localized uplift and increasing components of sediment deposition that progressively reduce relief towards the foreland.

The doubly-vergent Pyrenean orogenic wedge formed from Late Cretaceous to Early Miocene (~80-20 Ma) continental collision of Iberia and Eurasia (Figure 1) [*Sibuet et al.*, 2004] and accommodated moderate and variable shortening magnitudes (<165-80 km) along strike [*Muñoz*, 1992; *Vergés et al.*, 1995; *Teixell*, 1998; *Beaumont et al.*, 2000]. Existing datasets quantify the erosional exhumation in the range interior, the Axial Zone, and suggest that spatiotemporal variations in surface mass flux across the wedge and into the adjacent basins strongly impacted the development and architecture of the range [e.g. *Morris et al.*, 1998; *Fitzgerald et al.*, 1999; *Sinclair et al.*, 2005; *Whitchurch et al.*, 2011; *Fillon and van der Beek*, 2012]. In particular, the closure and abrupt reopening of the southern Ebro foreland basin is thought to play a major role in syn- and post-orogenic Pyrenean development [*Coney et al.*, 1996]. Although the history of deformation and sedimentation within and adjacent to the southern FTB wedge is well constrained [e.g. *Burbank et al.*, 1992a; *Hogan and Burbank*, 1996; *Vergés and Burbank*, 1996; *Rahl et al.*, 2011], the relationship with exhumation on the thin-skinned portion of the wedge remains poorly quantified. Zircon fission track samples from the southern Pyrenees have an inherited exhumation signal from the range interior [*Filleaudeau et al.*, 2011; *Whitchurch et al.*, 2011], but pilot apatite (U-Th)/He data from the region is reset [*Fillon et al.*, 2010]. This hints that lower temperature thermochronometers, such as fission tracks and (U-Th)/He in apatite, may be reset and record *in situ* (non-detrital) exhumation associated with cooling post-deposition.

In this study apatite fission track (AFT) thermochronology is used to quantify the spatiotemporal patterns of exhumation across an undocumented portion of the southern Pyrenean wedge. We compare this new exhumation record of the thin-skinned FTB margin with existing data from the range interior. Because sediment shed from the interior became incorporated into piggyback basins within the thin-skinned FTB, we differentiate between a detrital and a reset exhumation signal in sedimentary bedrock by comparing exhumation and deposition timing. The temperature sensitivity and spatial distribution of AFT data reveal that the Pyrenean orogenic wedge responded to crustal shortening through the processes of hinterland exhumation, erosion, basin sedimentation, and re-exhumation in response to deformation-driven uplift. We suggest that (a) most exhumation of the Pyrenean FTB appears to be related to taper adjustment by the orogenic wedge, although a post-orogenic base level lowering event may have excavated some areas and (b) climate may play an underappreciated role in the late stages of orogenesis.

II. GEOLOGIC SETTING

In the Early Cretaceous (~125 Ma), the Iberian plate rotated counterclockwise and began converging northwards with Europe (Figure 1) [*Sibuet et al.*, 2004]. Partial subduction of the Iberian lithosphere under the European plate and inversion of pre-existing extensional faults accommodated shortening along this plate boundary [*Vergés et al.*, 2002]. Major Pyrenean mountain building lasted from the Late Cretaceous to Early Miocene (~80-20 Ma) [*Sinclair et al.*, 2005], forming a wedge with a central Axial Zone and flanking thrust belt-foreland basin systems (Figure 2) [*Muñoz*, 1992]. Beginning at 36 Ma [*Costa et al.*, 2009], the southern Ebro foreland basin became closed, losing connection with the Atlantic and causing sediments shed from the exhuming Pyrenees to fill the basin and even bury the southern flank of the FTB to elevations of ~2.6 km [*Coney et al.*, 1996; *Fillon and van der Beek*, 2012]. Fluvial excavation of the southern FTB followed Ebro Basin capture by the Mediterranean 13-8.5 Ma [*Garcia-Castellanos et al.*, 2003; *Arche et al.*, 2010]. Rifting related to the opening of the Valencia Trough caused uplift of the southeastern margin of the Ebro Basin and eastern Pyrenees during the Neogene and Quaternary (<23 Ma) [*Lewis et al.*, 2000].

Pyrenean thrust belt structure, deformation timing, and spatial variations in shortening are well documented and relevant to the results of this study. Seismic reflection, balanced cross sections, and geodynamic models indicate maximum shortening of ~165-147 km in the central Pyrenees along the ECORS transect (Figure 2B) [*Beaumont et al.*, 2000; *Muñoz*, 1992]. Shortening decreases away from ECORS, with minimum estimates of ~125 km across the eastern Pyrenees [*Vergés et al.*, 1995] and 80 km across the western Pyrenees [*Teixell*, 1998]. The ECORS deep reflection seismic survey shows that the Axial Zone basement rocks are deformed into a crustal-scale duplex structure [*Muñoz*, 1992]. The uppermost thrust sheet of the duplex forms the Nogueres Zone that acts as the backstop for the southern, thin-skinned portion of the FTB. To the east, the structural equivalent is the Freser antiformal stack (Figure 3) [*Burbank et al.*, 1992b]. The thin-skinned portion of the FTB is widest in the central Pyrenees and consists of the Boixols, Montsec, and Sierres Marginales thrust sheets from north to south (Figure 2B, 3). Deformation across the central and eastern thin-skinned FTB lasted from the Late Cretaceous to Oligocene (~85-24 Ma). The south-central thrust sheets form an imbricate fan system that generally propagated southwards towards the foreland (Figures 2, 3) [*Vergés and Muñoz*, 1990], but some north-vergent and out-of-sequence thrusting is evident from cross-cutting stratigraphic relationships [e.g., *Burbank et al.*, 1992a; *Meigs et al.*, 1996; *Meigs and Burbank*, 1997, *Ramos et al.*, 2002]. In the eastern Pyrenees, the Vallfogona Thrust marks the southern boundary of the Cadi and Pedraforca thrust sheets [*Vergés et al.*, 2002]. Magnetostratigraphy and fault gouge dating constrain thrust sheet development in the eastern Pyrenees to a narrower time frame than the south-central Pyrenees, from ~54-37 Ma *[Burbank et al. 1992b, Capote et al., 2002, Haines, 2008]*.

Existing thermochronometer data quantify the broadest exhumation patterns across the Pyrenees (Figure 3). Paired zircon U-Pb geochronology and fission track thermochronology in the southern thrust belt-foreland basin found that convergence, shortening, and exhumation accelerated during the Late Cretaceous (~80 Ma) [*Filleaudeau et al.*, 2011] and that oblique convergence caused topography to develop diachronously along strike, from east to west between the Late Cretaceous and Miocene (~80-20 Ma) (Figure 1) [*Whitchurch et al.*, 2011]. Axial Zone Hercynian plutons exhumed most rapidly ~35-30 Ma in both the east [*Morris et al.*, 1998] and the south [*Fitzgerald et al.*, 1999], followed by slower exhumation starting at 30 Ma. The reduced exhumation from 30 Ma is attributed to base level change in the Ebro foreland basin, where syntectonic sediment infill reduced local relief [*Beamud et al.*, 2010]. ECORS transect thermochronometer data and discrete element modeling show an asymmetric exhumation pattern in the central Pyrenees [*Fitzgerald et al.*, 1999; *Sinclair et al.*, 2005]: exhumation migrated from north to south in response to the propagation of deformation and erosion across the pro-wedge. This asymmetric pattern caused orogenesis in the Pyrenees to end with syntectonic sediment blanketing of the southern range margin, pushing deformation from the FTB front back towards the pro-wedge hinterland, enhancing topography and accelerating erosion ~20 Ma in the Nogueres Zone [*Sinclair et al.*, 2005]. Remnants of this sediment blanket preserved in syntectonic basins on the southern thrust sheets record rapid cooling at ~50-40 Ma and ~30-25 Ma associated with source region exhumation in the Axial Zone [*Beamud et al.*, 2010; *Rahl et al.*, 2011]. Samples from the lowest elevations in the piggyback basins record partial fission track annealing <10 Ma, contemporaneous with fluvial excavation following Ebro Basin capture by the Mediterranean [*Beamud et al.*, 2010]. Finally, thermokinematic modeling of the Axial Zone low-temperature thermochronology data suggests that the sediment cover filled in the existing topography of the southern Pyrenees to elevations of ~2.6 km [*Fillon and van der Beek*, 2012].

III. APATITE FISSION TRACK THERMOCHRONOLOGY

Overview

Apatite fission track (AFT) thermochronology uses the formation and temperature-dependent retention of damage trails called fission tracks that accumulate in apatite grains from the fission decay of ^{238}U to reconstruct the cooling history of rocks in the uppermost crust [*Fleischer et al.*, 1975; *Gallagher et al.*, 1998]. Apatite grains retain fission tracks at temperatures below an effective closure temperature, dependent on composition (~110-120°C for fluorapatite) and cooling rate [*Ketcham et al.*, 1999]. In general, an AFT age, measured from the ratio of parent to daughter (^{238}U : fission tracks) concentrations, represents the time since the grain cooled from below its closure temperature [*Dodson*, 1973]. Fission tracks form with lengths of 14.5-16 μm [*Gleadow et al.*, 1986], but shorten (anneal) at temperatures within a partial annealing zone (PAZ) that occurs over a temperature window ~60°C below closure [e.g. *Gallagher et al.*, 1998].

Many apatite grains (~20-40) are analyzed in a sample, thus providing a distribution of fission track lengths and ages. The length distribution preserves a record of the thermal history of a sample as it cools below its closure temperature and through the PAZ [*Gleadow et al.*, 1986]. Summing the individual grain ages within each sample yields a pooled age [*Donelick et al.*, 2005]. A chi-squared test (χ^2) assesses the sample grain age variability [*Galbraith*, 1981]. A $P(\chi^2) > 5\%$ indicates minor grain age variability, and these samples are called concordant. A concordant sample pooled age represents the last time it cooled from closure temperature [*Brandon et al.*, 1998; *Galbraith*, 1981; *Green*, 1981]. A $P(\chi^2) < 5\%$ indicates significant grain age variability, or discordance, and the pooled age is considered less meaningful [e.g., *Green*, 1981].

Discordance may result from multiple component ages or heterogeneous mineral properties, especially in sedimentary rocks that can have multiple sediment sources [*Tagami and O'Sullivan*, 2005]. Fission track diameter (D_{par}) is a measure of grain solubility and a proxy for composition and thus is commonly measured to distinguish these properties [*Burtner et al.*, 1994; *Ketcham et al.*, 1999]. Applying a combination of component age analysis and thermal modeling is the most useful technique for determining the thermal history of discordant samples [*Barnes et al.*, 2006; *Barnes et al.*, 2008].

Sample Collection and Analysis

We collected bedrock samples from four across-strike transects of the central-eastern Spanish Pyrenees to determine the regional exhumation patterns across the southern FTB margin (Figure 3). These transects follow the balanced cross sections of Vergés [1999]. We targeted the major FTB structures, including the Cadi, Montsec, and Sierras Marginales thrust sheets, the Nogueres Zone, the Oliana anticline, and the Freser antiformal stack. We sampled Permian, Triassic, and Cretaceous sandstones and Eocene turbidites, sandstones, and conglomerates. We also sampled a Paleozoic schist north of the Freser antiformal stack and the Mount Louis-Andorra pluton exposed in the Axial Zone. We used standard techniques to isolate apatite grains and measure fission track ages, lengths, and D_{par} values (Appendix A). The fission track ages were determined using the laser ablation method (LA-ICP-MS) [*Donelick et al.*, 2005; *Hasebe et al.*, 2004].

Grain Age Analysis and Thermal Modeling

We applied both grain age analysis and thermal modeling to aid in interpretation of the AFT data (see details in Appendices B and C). For all discordant samples ($P(\chi^2) < 5\%$), we used binomial peak-fitting [*Galbraith and Green*, 1990] to identify the statistically significant age components with the software RadialPlotter [*Vermeesch*, 2008]. We classified sample grain-age distributions to assess the cooling history as (c.f. Brandon et al. [1998]): reset (R), mixed reset (MR), partially reset (PR), or detrital (D). R and MR samples have one or more component ages that are younger than the bedrock formation age. A PR sample contains component ages both younger and older than the sample formation age. D samples have one or more component ages that are older than sample formation age. In sedimentary samples, a D sample implies source region cooling, R and MR suggest *in situ* cooling, and a PR sample some mixture of both.

We used the thermal modeling software HeFTy [*Ehlers*, 2005; *Ketcham*, 2005] to constrain sample cooling histories consistent with the measured FT age, length, and D_{par} data. We simulated geologic processes such as formation, exhumation, burial, and re-exhumation (Figure 3 inset) by progressively incorporating time-temperature constraints on inverse models for each sample (see details Appendix B). We report time-temperature path envelopes that encompass the common merit values of 0.5 (good model fits) and 0.05 (acceptable model fits) from a Kuiper statistical test [*Ketcham*, 2005]. Because the study area was unaffected by Cenozoic volcanism or extension [e.g., *Vergés et al.*, 2002], we attribute recent thermochronometer-recorded cooling to erosional exhumation.

IV. RESULTS

Overview

We report AFT data for 18 bedrock samples from Cambrian through Eocene sandstones, conglomerates, schists, and granodiorites exposed across the southern Axial Zone and FTB of the Spanish Pyrenees (Figure 3). Sample grain age and track length yields range from maximum (40 ages, 200+ track lengths) to very poor (3 ages, 5 track lengths) with most (14 of 18) samples possessing robust results (>10 ages and track lengths). Sample pooled ages range from Late Cretaceous to Early Miocene (76.8-20.1 Ma) with mean track lengths from 15.12 to 12.85 µm implying fast to moderate cooling through the PAZ (Table 1). The pooled ages, identical within error to the more commonly reported central ages (Appendix C), suggest that all samples experienced enough exhumation during Pyrenean orogenesis to reset the AFT system. However, since most samples are discordant, we used thermal modeling and grain age analysis to evaluate this simple interpretation. No correlation between D_{par} and either track length or grain age within any of our samples indicates that sample discordance does not result from variable kinetic properties but instead likely reflects multiple age populations, although U loss could also play a role [*Brandon et al.*, 1998; *Ketcham et al.*, 1999]. All samples except one (WT1) have low mean D_{par} values (<1.6 µm), suggesting they contain thermally-sensitive fluorine-rich apatite [*Carlson et al.*, 1999] with fission tracks that survive heating to ~100ºC and partially anneal between 100-40ºC (Figures 4-7) [*Reiners and Brandon*, 2006].

Table 1. Apatite Fission Track Data[a]

Sample	Lat	Long	Elev, m	Fm Age, Ma	n	Ns, tracks	Dpar, µm	Area, cm^2	$\sum(P\Omega)$, cm^2	1σ $\sum(P\Omega)$, cm^2	ξ_{MS}	1σ ξ_{MS}	$P(\chi^2)$, %	Pooled Age, Ma ± 2σ	C. Age Class	MTL ± 2σ, µm (N_t, tracks)
								Eastern Transect (ET)								
ET1	42.27	2.16	823	99-54.8	40	356	1.48	1.08E-03	1.11E-04	8.55E-07	14.309	0.328	0.0	22.9+/- 2.6	PR	13.84 ± 2.82 (98)
ET2	42.29	2.16	854	99-54.8	27	120	1.25	5.81E-04	5.27E-05	9.68E-07	17.633	0.431	0.7	20.1 +/- 3.8	PR	14.66 ± 2.02 (52)
ET3	42.32	2.17	934	543-443	8	35	1.57	1.26E-04	8.03E-06	3.34E-07	14.279	0.328	5.8	31.0+/- 11	-	13.32 ± 2.90 (25)
								Central-Eastern Transect (CET)								
CET1	42.13	1.90	637	49-41.3	31	197	1.28	4.19E-04	5.52E-05	6.97E-07	16.821	0.415	0.4	30.0+/- 4.6	R	13.01 ± 2.96 (156)
CET2	42.28	1.85	1052	248-206	38	734	1.36	7.21E-04	2.70E-04	2.84E-06	17.491	0.428	0.2	23.7+/- 2.2	MR	13.60 ± 2.84 (182)
								Central-Western Transect (CWT)								
CWT1	42.06	1.31	472	37-33.7	40	939	1.55	1.09E-03	1.53E-04	1.15E-06	14.249	0.329	0.0	43.6+/- 3.6	PR	14.24 ± 3.10 (205)
CWT2	42.18	1.32	520	99-54.8	5	61	1.13	9.56E-05	1.99E-05	6.24E-07	17.396	0.426	41.8	26.7+/- 7.2	-	13.25 ± 2.88 (12)
CWT3	42.29	1.37	592	248-206	40	1643	1.52	1.74E-03	4.22E-04	3.20E-06	14.198	0.330	0.0	27.6+/- 2.0	R	14.18 ± 3.54 (202)
CWT4	42.30	1.37	578	290-248	40	155	1.56	1.03E-03	3.78E-05	2.57E-07	14.046	0.332	3.6	28.7+/- 4.8	R	14.06 ± 3.62 (26)
								Western Transect (WT)								
WT1	41.88	0.88	286	248-206	3	16	2.91	4.27E-05	2.17E-06	3.97E-08	13.957	0.334	48.8	51.2+/- 25.8	-	15.12 ± 0.46 (5)
WT2	42.01	0.88	336	248-206	8	119	1.44	9.12E-05	1.87E-05	2.91E-07	13.964	0.334	0.0	44.2+/- 8.4	MR	14.67 ± 3.38 (24)
WT3	42.06	0.89	364	144-65	39	3075	1.27	1.13E-03	3.38E-04	3.74E-06	16.990	0.418	0.0	76.8+/- 5.0	PR	12.95 ± 3.60 (204)
WT4	42.16	0.88	504	99-54.8	17	205	1.36	3.11E-04	3.51E-05	5.66E-07	17.113	0.421	0.0	49.7+/- 7.6	MR	12.85 ± 3.06 (13)
WT5	42.15	0.81	766	54.8-33.7	15	190	1.37	3.38E-04	2.73E-05	6.25E-07	17.183	0.422	0.0	59.5+/- 9.6	D	13.09 ± 2.56 (37)
WT6	42.16	0.78	1039	54.8-33.7	37	2422	1.29	1.45E-03	4.37E-04	5.16E-06	17.300	0.424	0.0	47.7+/- 3.2	PR	13.93 ± 2.94 (200)
WT7	42.33	1.07	611	248-206	40	953	1.56	1.43E-03	2.44E-04	1.48E-06	13.995	0.333	0.0	27.3+/- 2.2	MR	14.49 ± 2.80 (201)
								Axial Zone (AZ)								
AZ1	42.51	1.57	1593	354-248	40	557	1.42	1.40E-03	1.72E-04	1.77E-06	14.147	0.331	0.0	22.8+/- 2.2	MR	14.17 ± 3.82 (133)
AZ2	42.51	1.55	1134	354-248	40	471	1.41	1.44E-03	1.37E-04	1.23E-06	14.097	0.332	0.0	24.2+/- 2.6	MR	13.64 ± 3.42 (136)

[a]ET, Eastern Transect; CET, Central-Eastern Transect; CWT, Central-Western Transect; WT, Western Transect; Fm, Formation; n, number of grains measured; Dpar, mean maximum diameter of fission track etch figures parallel to the c-axis; Ns, number of spontaneous tracks counted; Area, grain area analyzed; Σ(PΩ), area-weighted 238U/43Ca, summed over n grains per sample; σ, standard deviation; ξMS, zeta calibration factor; P(X2), chi-squared probability; MTL, mean track length measured from Nt tracks.

Below, we summarize our results along the four FTB transects from east to west in the direction of increased shortening [Vergés et al. 2002], followed by the Andorra-Mount Louis pluton in the Axial Zone. Samples are numbered from south to north and representative thermal model results are shown in Figures 4-7. We focus on the timing of most recent rapid cooling history of each sample based on the statistically good thermal model fits [*Ketcham*, 2005].

Eastern Transect (ET)

We report results from three samples along the eastern transect (Figure 4). Two samples (ET1, ET2) are from Late Cretaceous-Paleocene sandstone units of the Garumnian Formation exposed in the Freser antiformal stack. They have pooled ages of 23-20 Ma and moderate mean track lengths (13.8-14.7 μm). Both samples are discordant and considered partially reset. Modeling indicates that sample ET1 cooled rapidly through 100°C between 25-20 Ma, whereas sample ET2 produced no model fits. Sample ET3 is from quartz-rich schist exposed on the hanging wall of the Ribes-Camprodon fault, north of the Freser antiformal stack. This sample has poor data quality (8 grains, 35 track lengths) with modeling that suggests rapid cooling began from ~90°C 38-18 Ma.

Central-Eastern Transect (CET)

We analyzed two samples from the Cadi thrust sheet south and north of the Pedraforca thrust sheet along the central-eastern transect (Figure 5). Sample CET1 is from the middle Eocene Campdevanol Formation on the Vallfogona thrust hanging wall. It has a pooled age of 30 ± 4.6 Ma and a mean track length of 13.01 ± 2.96 μm. CET1 is reset and slowly cooling through PAZ temperatures after 38-24 Ma. The northern sample (CET2) is from the lower Triassic Buntsandstein Formation [Gradstein et al. 2004] and has a pooled age of 23.7 ± 2.2 Ma and a mean track length of 13.6 μm. The age components this sample is mixed reset and acceptable thermal model fits indicate recent cooling through ~110°C 27-21 Ma.

Central-Western Transect (CWT)

We analyzed four samples along the central-western transect (Figure 6). Sample CWT1 is from the southern limb of the Oliana anticline and has a pooled age of 43.6 ± 3.6 Ma and mean track length of 14.24 ± 3.1 μm. This sample is partially reset and cooled rapidly through PAZ temperatures ~18-16 Ma. Sample CWT2 is from the Cretaceous-aged sandstone of the Garumnian Formation and has a pooled age of 26.7 ± 7.2 Ma and mean track length of 13.25 ± 2.88 μm. Modeling suggests this sample cooled from ~90°C between 34-15 Ma. Samples CWT3 and CWT4 are from Triassic and Permian sandstones in the footwall of the Boixols back thrust and have similar pooled ages (27.6-28.7 Ma) and mean track lengths and (14.1-14.2 μm). Both samples are reset. Sample CWT3 cooled below 90°C between 25-24 Ma. CWT4 is less constrained, but cooling rapidly between 36 and 18 Ma.

Western Transect (WT)

We report seven samples on the western transect (WT), which is equivalent to the ECORS profile (Figures 2, 7). The southernmost sample (WT1) is from the Triassic Keuper Formation exposed in the Sierras Marginales thrust sheet hanging wall. This sample is concordant, but because it has poor FT data quality (3 ages, 16 track lengths), permissible model paths define a broad time period (64-32 Ma) for rapid cooling from closure temperatures. Sample WT2 is also from the Triassic Keuper Formation exposed on the Montsec thrust sheet. This mixed reset sample has a pooled age of 44.2 ± 8.4 Ma, a mean track length of 14.67 ± 3.38 μm, and rapidly cooled 18-13 Ma from ~100°C. Sample WT3 is from the Cretaceous Marbore sandstone on the Montsec thrust sheet. It is partially reset and cooled slowly through the PAZ 90-45 Ma. Samples WT4-6 form an ~500 m elevation transect within the Graus-Tremp Basin on the Montsec thrust sheet. They have pooled ages of 47.7-59.5 Ma and mean track lengths that increase up section, suggesting that the lower elevation samples from the profile spent more time in PAZ temperatures. WT4, a mixed reset sample from the Late Cretaceous-Paleocene Garumnian Formation at the profile base, began cooling 61-37 Ma. WT5, a detrital sample from Eocene sandstone in the middle of the profile, began cooling 71-53 Ma. Partially reset sample WT6, from the highest elevation, rapidly cooled from above PAZ temperatures between 52-41 Ma. Thermal models of WT5 and WT4 indicate slower cooling through PAZ temperatures. Finally, the northernmost sample (WT7) is from a Triassic sandstone in the Nogueres Zone and is mixed reset. WT7 cooled rapidly through closure temperatures 29-23 Ma.

Andorra-Mount Louis Pluton

Two Axial Zone granodiorite samples from the Andorra-Mount Louis pluton have similar pooled ages (24.2-22.8 Ma), mean track lengths (14.2-13.6 μm), and D_{par} values (1.4 μm). Both samples began to cool rapidly 25-20 Ma.

V. DISCUSSION

AFT Cooling and Wedge-Top Deposition

We determine whether AFT cooling on the southern FTB margin records an inherited exhumation signal from Axial Zone or *in situ* exhumation by comparing the timing of exhumation with wedge top deposition (Figure 8). This comparison yields two distinct subsets within our data: (1) exhumation contemporaneous with deposition and (2) exhumation post-dating deposition. Case 1 indicates an inherited cooling signal, present in sedimentary units where the apatite grains were not fully reset by post-depositional burial and instead retain a record of cooling associated with their earlier erosion from the Axial Zone source region (red stars, Figures 3-8). This is the case for four of our five samples from the Montsec thrust sheet, including all of the Graus-Tremp Basin samples (Figure 8). There is a similar inherited signal in granitic cobbles from related syntectonic basins preserved on the Montsec and Boixols thrust sheets and Nogueres Zone (blue stars, Figure 3, 8) [*Beamud et al.*, 2010; *Rahl et al.*, 2011]. The only other location that retains a source region exhumation signal is the leading edge of the Sierras Marginales thrust sheet. All other samples from the southern FTB structures fit the second case because they experienced *in situ* exhumation great enough to reset the AFT system post-deposition. While the possible exhumation timing of our Sierras Marginales sample is broad, if we refine it to the deposition age, it records a detrital signal of the rapid exhumation in response to antiformal stacking in the southern Axial Zone at ~30 Ma.

Interpreted Exhumation History

The Late Eocene was a time of abrupt change in the southern Pyrenees. Thrusting and duplex formation rapidly exhumed the south-central Axial Zone ~35 Ma [*Muñoz*, 1992; Morris *et al.*, 1998; *Fitzgerald et al.*, 1999; *Beaumont et al.*, 2000; *Sinclair et al.*, 2005]. Ebro foreland basin closure [*Burbank et al.*, 1992a; *Verges and Burbank*, 1996] caused drainage system reorientation from dominantly orogen parallel to orogen transverse (Figure 9) [*Whitchurch et al.*, 2011]. The only AFT data on the thin-skinned portion of the FTB recording pre-35 Ma exhumation are syntectonic piggyback basin sediments (white rimmed symbols, Figures 3-8). In the Axial Zone, the AFT data with a pre-35 Ma exhumation signal are clustered towards the north and east (Figure 3, 9A).

The overall distribution of pre-35 Ma exhumation reflects the patterns of along- and across-strike tectonic development during Pyrenean orogenesis (Figure 9A). Exhumation started in the eastern Pyrenees in response to oblique convergence driving uplift and topographic growth (Figure 1). Exhumation subsequently decreased in the eastern Pyrenees, preserving a record of older exhumation as uplift shifted along strike to the central Pyrenees during the Early to Middle Eocene ~55-40 Ma [*Whitchurch et al.*, 2011]. While exhumation in the central Pyrenees began before 35 Ma, asymmetric convergence between the pro-wedge and retro-wedge drove exhumation southward over time [*Sinclair et al.*, 2005], removing most of the pre-35 Ma signal from the southern Axial Zone. Subsidence within the Graus-Tremp Basin and equivalent syntectonic basins generated enough accommodation space to preserve the earlier erosion signal in detrital apatites from the Axial Zone source region [this study; see also *Beamud et al.*, 2010; *Rahl et al.*, 2011], a signal that is not present anywhere else on the thin-skinned FTB. In this way, the hinterland and thin-skinned FTB components of the orogenic wedge functioned together to redistribute mass during shortening in response to plate convergence.

Exhumation Magnitudes

We estimate exhumation magnitude on the FTB based on whether AFT sample ages are reset after deposition in our samples. Exhumation magnitudes are calculated assuming a paleogeothermal gradient of ~30°C/km [after *Beamud et al.*, 2010], a closure temperature of 100ºC, and a 20ºC surface temperature. The data suggest exhumation magnitudes did not exceed ~2.7 km in the interior of the Montsec thrust sheet or on the Sierras Marginales hanging wall (samples WT2-5, 7). This is consistent with structural data that estimate 0.5-1 km of material has been removed from the top of the Graus-Tremp basin since 28 Ma [*Meigs and Burbank*, 1997]. Our results also suggest that syntectonic sediment shed off the eroding Axial Zone, estimated from inverse thermo-kinematic modeling to reach elevations of ~2.6 km during the Late Eocene-Early Oligocene (~40-30 Ma) [*Fillon and van der Beek*, 2012], likely did not exceed ~3 km elevation. If the syntectonic infill exceeded this elevation, Miocene fluvial excavation may have reset the lowest elevation sample from the Sierras Marginales thrust sheet (WT1, 285 m elevation).

Tectonics, Climate, and Exhumation

The majority of AFT thermochronometer-recorded cooling from the southern Pyrenean FTB resulted from *in situ* exhumation (star-filled circles, Figures 3-9). This exhumation occurred after 35 Ma, despite deformation in the thin-skinned portion of the FTB beginning at least 65 Ma [*Ardevol et al.*, 2000]. We assess whether the *in situ* exhumation is related to near-surface deformation by comparison with exposed stratigraphic relationships and $^{40}Ar/^{39}Ar$ fault gouge dating in the southern Pyrenees [e.g. *Meigs et al.*, 1996; *Rahl et al.*, 2011]. For example, final motion on the Vallfogona thrust in the eastern Pyrenees (Figure 3) generated a progressive unconformity in the syntectonic Solsona foreland basin sequence 36-30 Ma [*Verges and Burbank*, 1996]. Our modeling indicates that rapid exhumation occurred contemporaneously on the Vallfogona thrust at 34-29 Ma (Figure 5). Therefore, we interpret the rapid exhumation to an erosional response to thrust-driven uplift.

In other cases, the recorded rapid exhumation phases occurred after major fault motion ceased. Upper Eocene syntectonic conglomerates onlap thrusts in the Nogueres Zone and authigenic illite in a minor overturned proximal thrust is ~56 Ma [*Rahl et al.*, 2011]. Two of our AFT samples cooled rapidly (>20°C/Myr through the PAZ) between 29-21 Ma in the Nogueres Zone, contemporaneous with AFT-recorded 26-17 Ma rapid cooling in nearby Carboniferous volcanic rocks [*Sinclair et al.*, 2005]. Instead of being related to earlier thrusting episodes, this Late Oligocene to Early Miocene exhumation may represent a response to underplating and antiform growth that generated significant erosion and increased sediment flux to the Ebro Basin [*Sinclair et al.*, 2005]. Samples from the Freser antiformal stack and from north of the Pedraforca thrust sheet record contemporaneous exhumation between 25-20 Ma and 27-21 Ma, respectively. These structures occupy a similar structural position to those in the Nogueres Zone at the transition between the Axial Zone and southern FTB (Figure 8).

Late stage (25-20 Ma) syn-orogenic exhumation in the Pyrenees could be caused by either exhumation commensurate with tectonic deformation and stable climate, or exhumation coincident with deformation and enhanced by climate change. Antiformal stack formation may have occurred synchronously along strike (Figure 9), coevally or immediately following the last phase of shortening on the southern thrust sheets after ~24.7 Ma [*Meigs et al.*, 1996]. Loading by the syntectonic sediment sourced from the Axial Zone at this time buried and stabilized the outboard FTB structures [*Coney et al.*, 1996], possibly causing deformation to shift towards the hinterland [this paper; *Jolivet et al.*, 2007]. This would have allowed the orogenic wedge to rebuild taper through underplating and thrusting, accommodating the final phase of convergence [*Beaumont et* *al.*, 2000]. This idea is supported by existing thermochronometer datasets and numerical models that suggest uplift from antiformal stacking drove rapid exhumation in the south-central Pyrenees during the Early Miocene [*Sinclair et al.*, 2005; *Gibson et al.*, 2007; *Jolivet et al.*, 2007].

Alternatively, a regional or global shift to warmer, wetter conditions could have initiated an exhumation pulse in the Axial Zone. Global climate in the Miocene is thought to be relatively warm and arid, peaking with the Middle Miocene climatic optimum [*Zachos et al.*, 2001]. However, recent investigations into the major element geochemistry of Early Miocene paleosols from the north-central Ebro Basin suggest that the regional climate was already subhumid to humid, with considerably more precipitation than the earlier arid to semiarid climate during the Late Oligocene [*Cabrera et al.*, 2002; *Hamer et al.*, 2007]. A shift to wetter, more erosive climate conditions poses another explanation for our observation of uniform along-strike exhumation ~25-20 Ma at the transition between the Axial Zone and thin-skinned southern FTB in addition to synchronous wedge adjustment across a structurally variable FTB.

Post-Orogenic Exhumation

Two samples from the central FTB record the youngest, post-orogenic exhumation in the Pyrenees (Figure 9D). Syntectonic conglomerates on the eastern margin of the central thrust sheets indicate Montsec thrust motion and folding of the Oliana anticline ~40-25 Ma [*Burbank et al.*, 1992a; *Vergés and Muñoz*, 1990]. Middle Eocene syntectonic conglomerates also bracket deformation to younger than ~45 Ma on the Montsec thrust west of sample WT2 [*Meigs and Burbank*, 1997]. However, model results show that the Oliana anticline and Montsec thrust sheet hanging wall both experienced rapid exhumation during the Miocene (<23 Ma) (Figures 6, 7). This suggests a period of erosion that post-dates active shortening. Several post-orogenic factors could be responsible for this exhumation. Basin modeling [*Garcia-Castellanos et al.*, 2003], seismic imaging of the Ebro delta [*Urgeles et al.*, 2010], and paleo-topographic signals within thermochronometer data [*Fillon and van der Beek*, 2012] imply that capture of the paleo-Ebro River by the Mediterranean Sea (at ~13-8.5 Ma) caused regional base level lowering and triggered excavation of the sediment blanket that buried both structures. One of our Montsec thrust sheet samples exhumed between 21 and 10 Ma and may corroborate these conclusions with direct evidence from the excavated region. However, the Oliana anticline exhumation occurred before this base level lowering event at 18-16 Ma. Thermo-kinematic modeling of thermochronometer data from the Axial Zone ruled out climate change as an important factor in the post-orogenic evolution of the Pyrenees [*Fillon and van der Beek*, 2012]. Finally, Late Oligocene-Early Miocene tilting near the southeast margin of the Ebro Basin, caused by lithospheric extension and thinning, coeval with opening of the Valencia Trough, may also enhance exhumation along large areas paralleling the range [*Lewis et al.*, 2000]. More detailed sampling and combined AFT and (U-Th)/He dating in apatite (closure temperature ~70ºC [*Farley*, 2000]) could test if this Early Miocene exhumation event is robust.

Summary and Comparison with Other Orogens

We suggest that oblique convergence and orogenic wedge adjustment played an important role in the spatiotemporal pattern of exhumation in the Axial Zone and southern Pyrenean FTB. However, surface processes such as the distribution and magnitude of sediment flux, burial of the FTB margin, foreland drainage basin reorganization, and climate-enhanced erosion modified this pattern. These broad components of Pyrenean structural and topographic development are consistent with the deformation, erosion, and sedimentation histories of other orogens. For example, stream capture can generate hundreds of meters of incision in the tectonically quiescent Appalachians [*Prince et al. 2011*], analogous to the post-orogenic incision that followed Ebro Basin capture by the Mediterranean. Duplex development and climate-driven erosion are important mechanisms for orogenic wedges to accommodate shortening and adjust their taper during mountain building. These mechanisms have been recognized as important during the Sevier orogeny in the western US [*DeCelles and Mitra*, 1995; *Mitra and Sussman*, 1997] as well as within portions of the Himalayas [*Bollinger et al.*, 2006; *Mitra et al.*, 2010; *Thiede et al.*, 2005] and the central Andes [*McQuarrie and DeCelles*, 2001; *McQuarrie et al.*, 2008].

VI. CONCLUSIONS

This study documents Cenozoic exhumation across the southern flank of the Pyrenean orogenic wedge with 18 new bedrock apatite fission track (AFT) samples. Comparison between the AFT cooling histories and sample deposition timing differentiates between samples that record inherited exhumation from the range interior (Axial Zone) or *in situ* exhumation. The Graus-Tremp syntectonic piggyback basin sediments record Axial Zone exhumation ~70-40 Ma, consistent with detrital exhumation signals present in AFT samples from other south Pyrenean piggyback basins [*Beamud et al.*, 2010; *Rahl et al.*, 2011]. The Sierras Marginales and Montsec thrust sheets record Axial Zone exhumation ~90-30 Ma. At these locations on the thin-skinned FTB, the inherited Axial Zone exhumation signal demonstrates that sediment burial and subsequent exhumation did not exceed ~3 km. Other thin-skinned FTB structures have reset cooling histories, recording *in situ* exhumation in excess of ~3 km. The Cadi thrust sheet exhumed from 34-29 Ma, contemporaneous with its final phase of deformation at 36-30 Ma. Reset cooling ages from the Oliana anticline and Montsec thrust sheet hanging wall reflect post-tectonic exhumation 20-10 Ma, perhaps in response to fluvial incision from abrupt foreland base level change and/or regional tilting coeval with Valencia Trough extension. Basement rocks at the transition from the thin-skinned FTB to the crustal-scale duplex of the Axial Zone record exhumation along the entire strike of the central-eastern FTB at 25-20 Ma. This rapid exhumation post-dates surface-breaking faults and may result from (a) antiformal stack development, previously noted in the Nogueres Zone of the central Pyrenees [*Sinclair et al.*, 2005] and/or (b) a shift to more humid climate conditions in the Early Miocene [*Hamer et al.*, 2007]. If exhumation is in response to uplift, deformation retreating from the thrust front to the interior of the orogen may relate to loading from erosional debris shed by the Axial Zone that accumulated on the southern FTB and foreland basin.

FIGURES

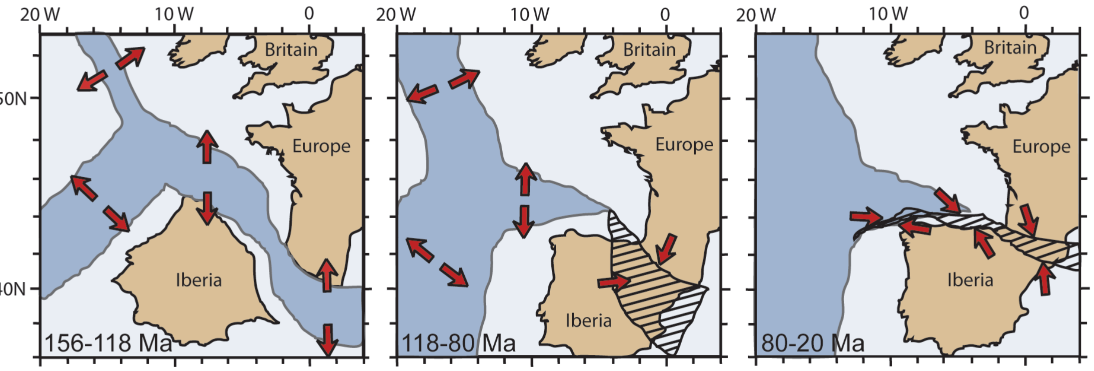

Figure 1. Kinematically restored plate motions based on paleomagnetic data with Europe fixed [Simplified from *Sibuet et al.*, 2004]. Arrows indicate relative plate motion directions. Hachured regions show where compression occurred and dark blue represents ocean basin.

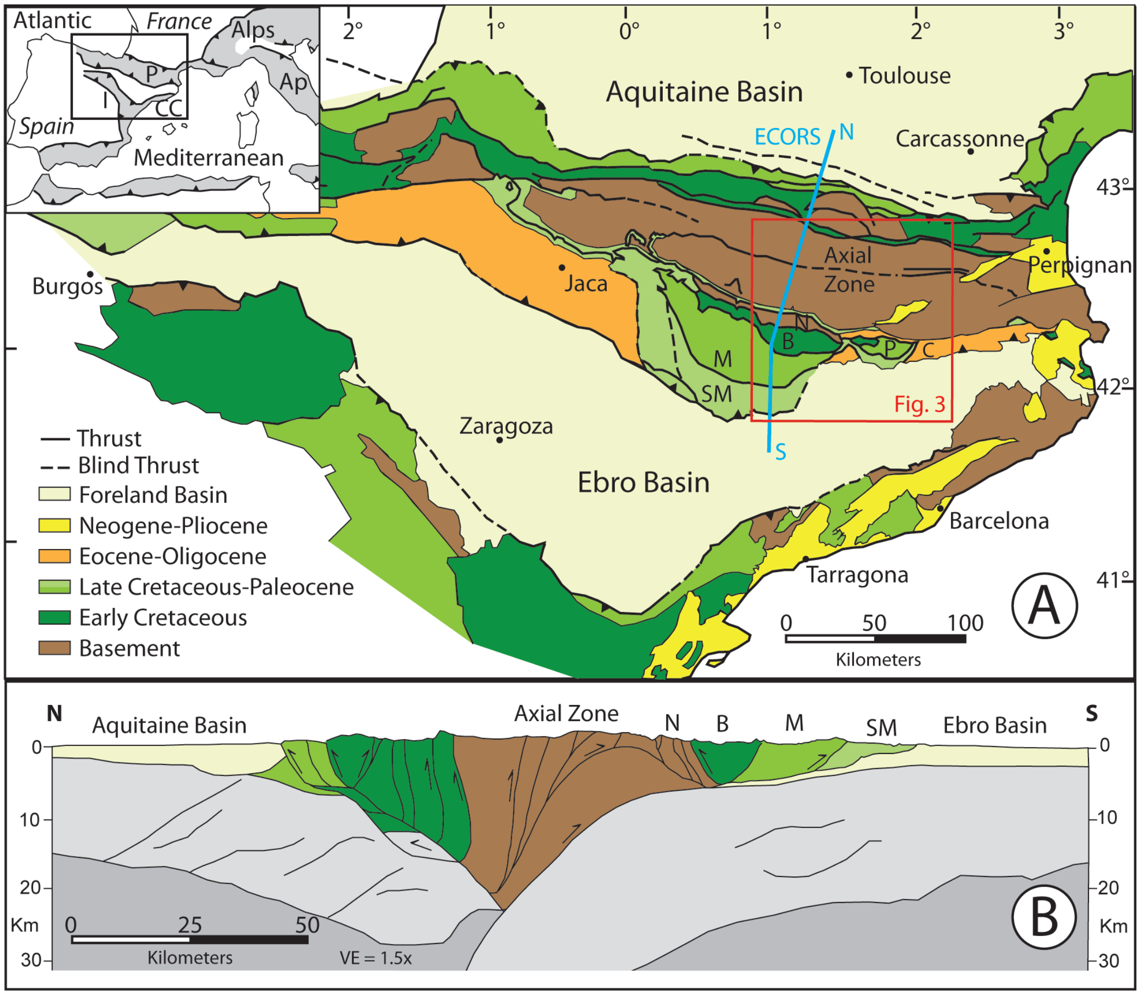

Figure 2. Geology of northeastern Iberia. (A) Simplified geologic map for the Pyrenees and surrounding regions [Modified from *Vergés and Burbank*, 1996]. Inset shows location and regional geographic context: Ap, Apennines; CC, Catalan Coastal Ranges; P, Pyrenees. Southern thrust sheets: B, Boixols thrust sheet; C, Cadi thrust sheet; M, Montsec thrust sheet; N, Nogueres Zone; P, Pedraforca; SM, Sierras Marginales. VE, vertical exaggeration. Red box is the study area and the blue line indicates the ECORS seismic profile [*Muñoz*, 1992]. (B) Crustal scale cross section along the ECORS transect (location in A) [modified from *Beaumont et al.*, 2000]. Note the bivergent wedge geometry and central duplex vs. marginal thin-skinned FTB structures of the Pyrenees.

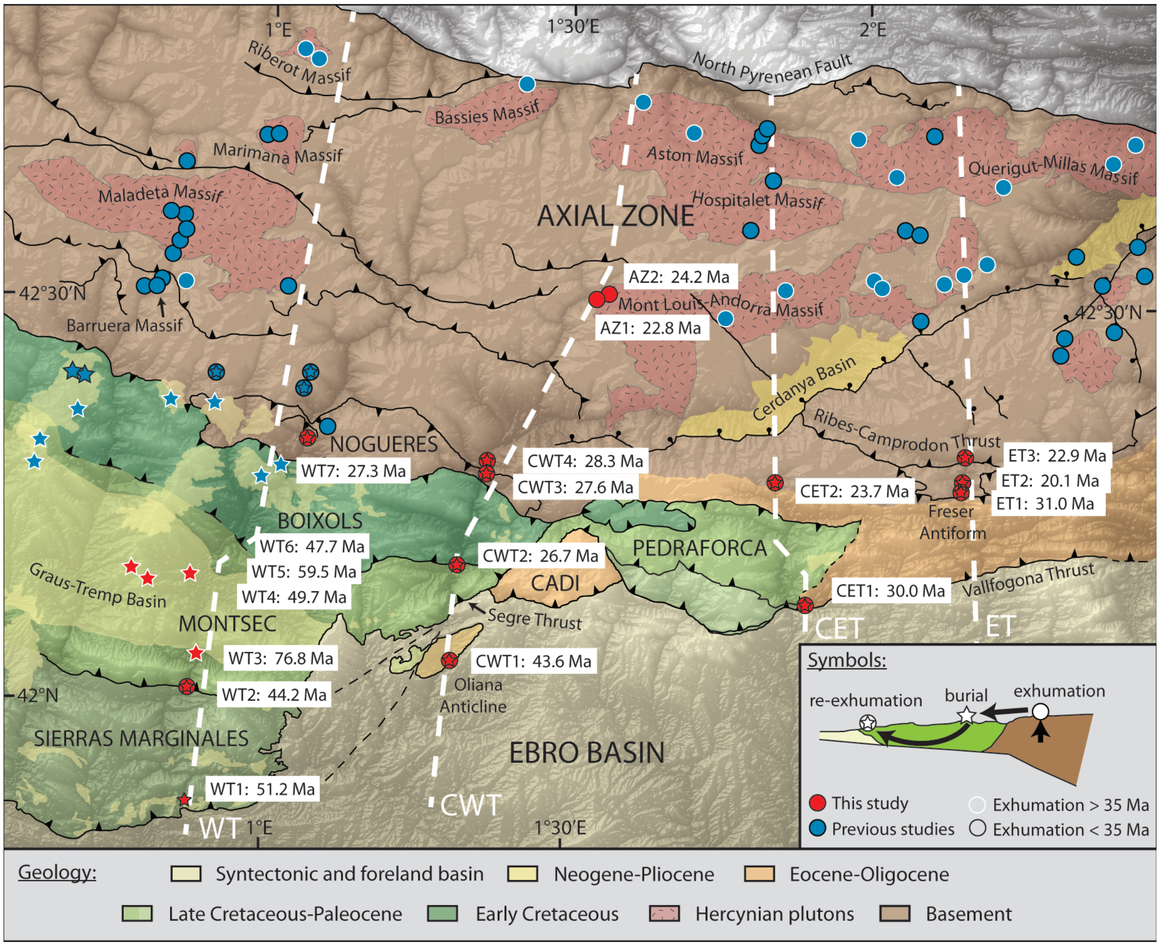

Figure 3. Topography, geology, and apatite fission track thermochronology data of the central-eastern Pyrenees. This synthesis highlights new and published bedrock apatite fission track (AFT) data within 10 km of the four transects. Inset shows our sample classification scheme, based on thermal model exhumation timing (white or black rim), location relative to where the sample most recently exhumed from AFT closure temperature (circle, star, or circled star; see discussion text for details), and dataset source (red or blue) [*Morris et al.*, 1998; *Fitzgerald et al.*, 1999; *Gibson et al.*, 2007; *Jolivet et al.*, 2007; *Gunnell et al.*, 2009; *Beamud et al.*, 2010]. Note that AFT pooled age, shown in white boxes alongside the sample number, and exhumation timing are not correspondent for discordant samples. WT, western transect; CWT, central western transect; CET, central eastern transect; ET, eastern transect. Geologic units generalized from Mapa Geologic de Catalunya [2003] and topography is the 30 m ASTER GDEM (http://asterweb.jpl.nasa.gov/gdem-wist.asp).

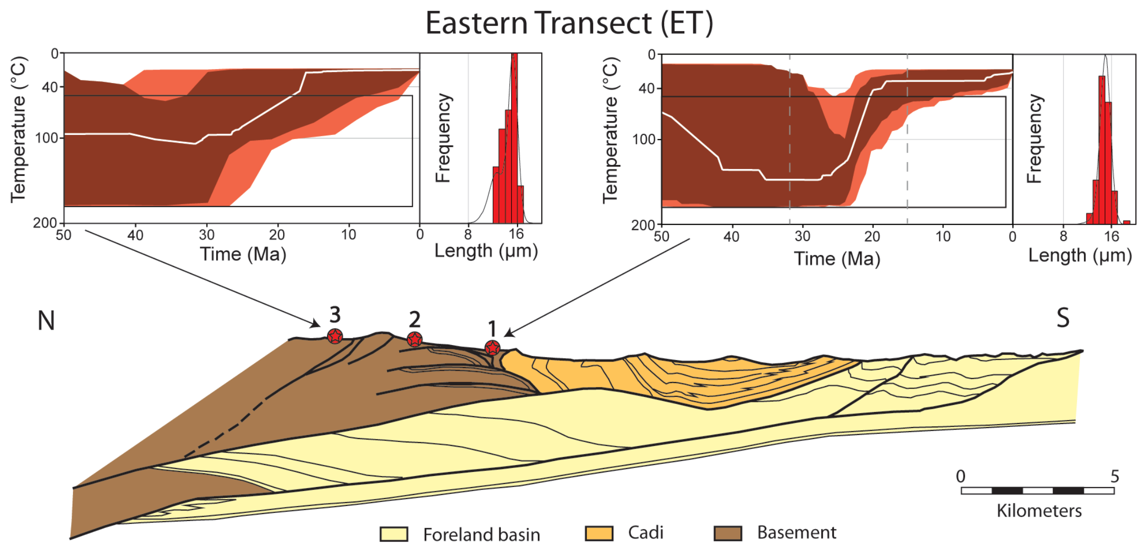

Figure 4. Structure of the eastern study transect (ET, location in Figure 3) [simplified from *Vergés*, 1999], numbered bedrock apatite fission track sample locations (symbol description in Figure 3 inset), and selected permissible time-temperature histories modeled with HeFTy [*Ketcham*, 2005]. Thermal envelopes show the range of good (dark red) and acceptable (light red) model fits. The white line is the best fit model path. Black boxes are modeling constraints (see methods for details). Horizontal gray lines highlight the partial annealing zone. Dashed vertical lines represent sample component ages determined using RadialPlotter [*Vermeesch*, 2008] (Appendix C). The track length distribution (red bars) and best fit model (line) are shown in the right panels.

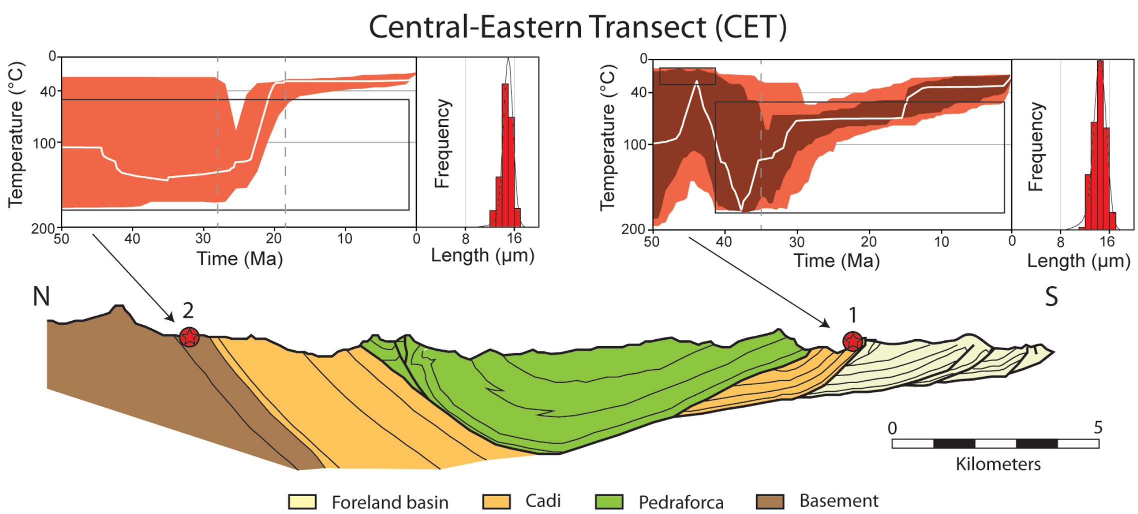

Figure 5. Structure of the central-eastern transect (CET, location in Figure 3), bedrock apatite fission track sample locations, and associated thermal modeling results. See Figure 4 caption for details.

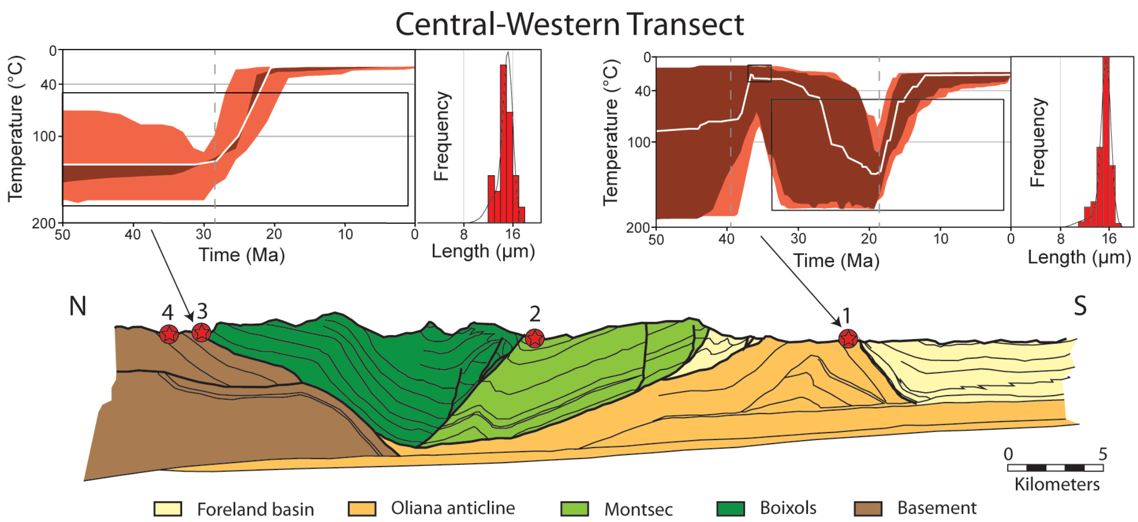

Figure 6. Structure of the central-western transect (CWT, location in Figure 3), bedrock apatite fission track sample locations, and associated thermal modeling results. See Figure 4 caption for details.

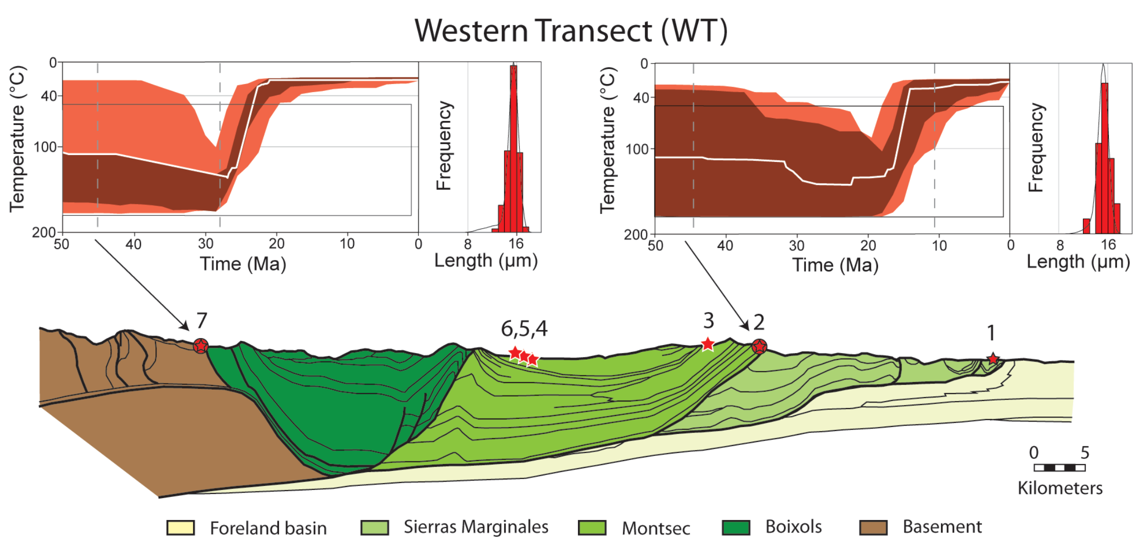

Figure 7. Structure of the western transect (WT, location in Figure 3), bedrock apatite fission track sample locations, and associated thermal modeling results. Structurally equivalent to the ECORS profile. See Figure 4 caption for details.

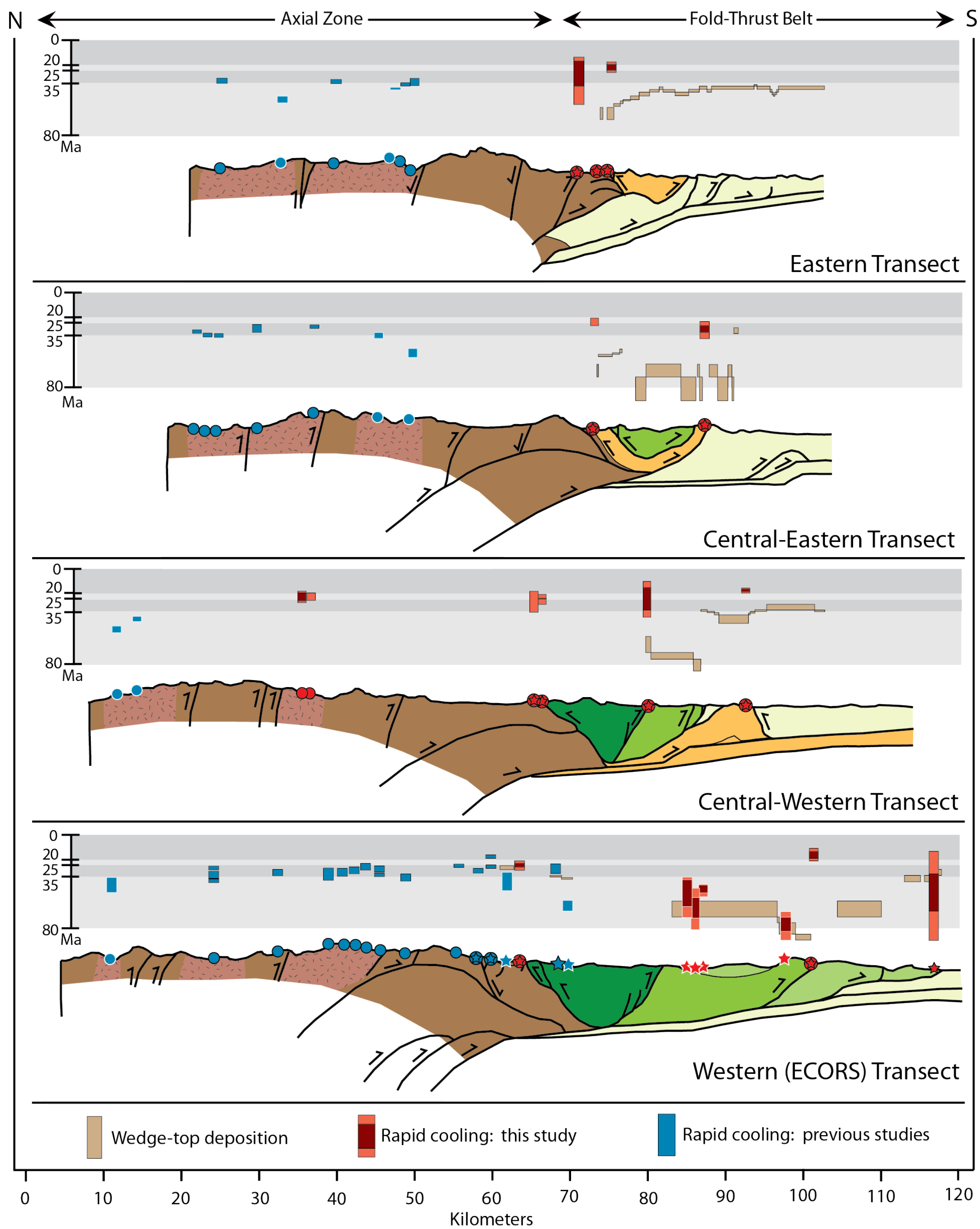

Figure 8. Simplified cross sections [from *Vergés*, 1999] along the four studied transects shown in Figures 3-7 synthesizing existing exhumation and sedimentation timing data across the central-eastern Spanish Pyrenees [*Beamud et al.*, 2010; *Fitzgerald et al.*, 1999; *Gibson et al.*, 2007; *Gunnell et al.*, 2009; *Jolivet et al.*, 2007; *Morris et al.*, 1998; *Rahl et al.*, 2011; *Sinclair et al.*, 2005]. Overlap between timing of rapid cooling and deposition means the samples retain an inherited exhumation signal from the Axial Zone source

region. Onset of rapid cooling from samples in this study is shown from the acceptable (red) and good (dark red) fit thermal model envelopes (e.g., Figures 4-7). Cross sections extend southward from the North Pyrenean Fault to the Ebro Basin. See Figure 3 inset for sample symbol descriptions. Gray bars highlight the time windows shown in Figure 9.

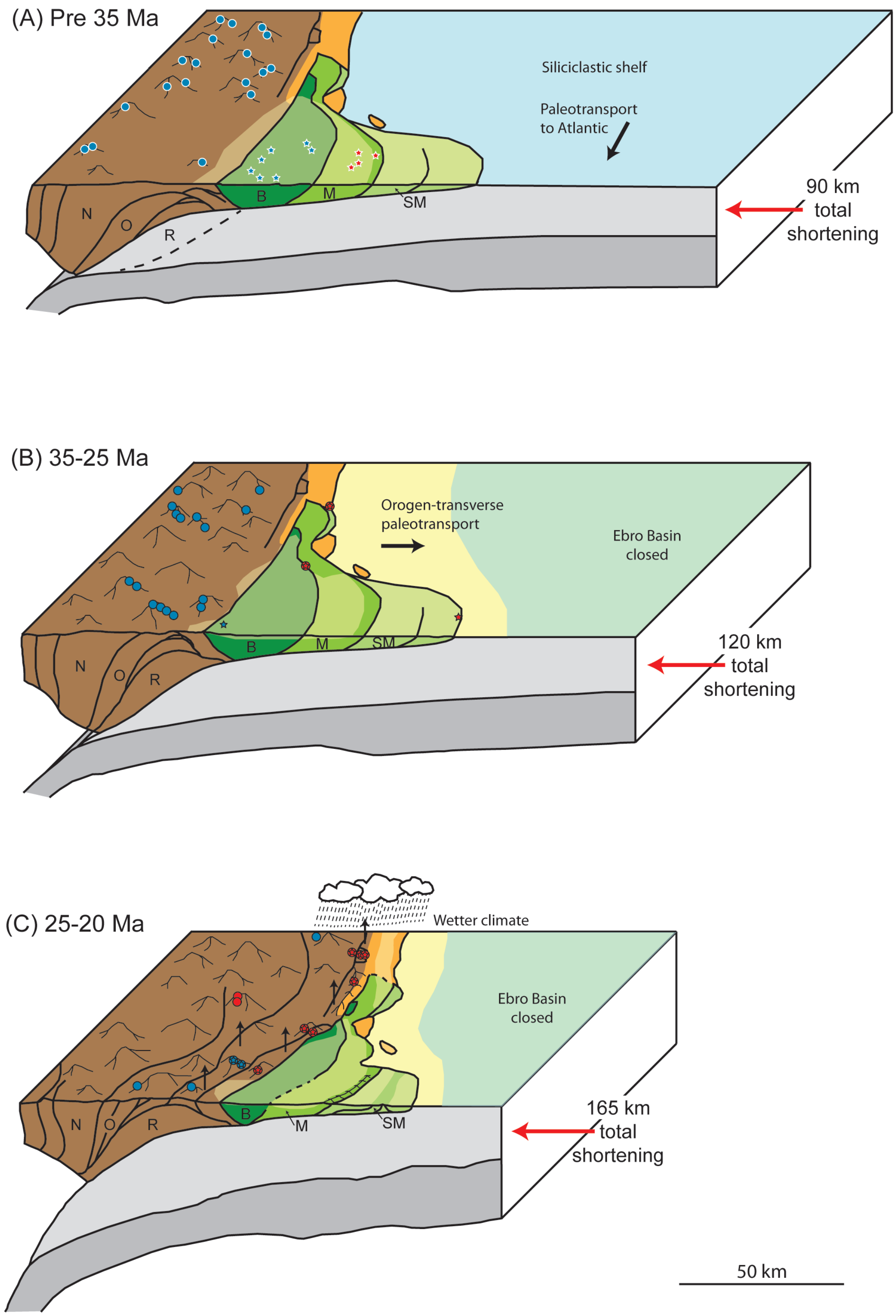
(A) Pre 35 Ma
Siliciclastic shelf
Paleotransport
to Atlantic
B
M
SM
N
O
R
90 km
total
shortening
(B) 35-25 Ma
Orogen-transverse
paleotransport
Ebro Basin
closed
B
M
SM
N
O
R
120 km
total
shortening
(C) 25-20 Ma
Wetter climate
Ebro Basin
closed
B
M
SM
N
O
R
165 km
total
shortening
50 km

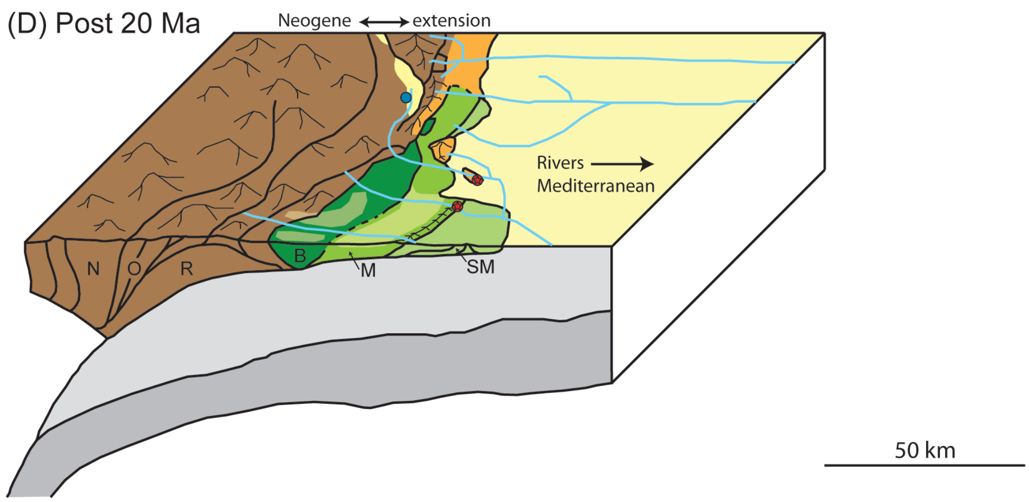

Figure 9. Summary of the syn- to post-orogenic evolution of the central-eastern Spanish Pyrenees. The Axial Zone develops diachronously from east to west [*Whitchurch et al.*, 2011] and north to south in the central Pyrenees [*Fitzgerald et al.*, 1999]. Closure of the Ebro Basin ~35 Ma causes syntectonic sediments to bury the southern thrust sheets, forcing the wedge to deform internally to rebuild taper and accommodate shortening. Fluvial excavation follows when the basin connects with the Mediterranean ~13-8.5 Ma [*Garcia-Castellanos et al.*, 2003]. N-S cross sectional view of the structural evolution of the southern orogenic wedge and total shortening estimates for the ECORS transect from Beaumont et al. [2000]. For the key to AFT sample location symbols, see Figure 3. Axial Zone antiformal stack thrust sheets: N-Nogueres, O-Orri, R-Rialp. Southern thrust sheets: B-Boixols, M-Montsec, SM-Sierras Marginales.

Appendix A: Analytical Procedures

All AFT analyses were performed at Apatite to Zircon, Inc. Samples were crushed and sieved to sand-sized particles, then apatite grains were isolated using standard gravimetric and magnetic mineral separation techniques [*Donelick et al.*, 2005]. Grains were mounted in epoxy resin, cured at 90°C for 1 hr, and then polished to expose the internal surfaces of the grains. Mounts were then immersed in 5.5N HNO_3 for 20 seconds at 21°C to reveal natural fission tracks that intersected the polished grain surface. Samples were irradiated with ^{252}Cf to facilitate fission track length measurement [*Donelick and Miller*, 1991]. Fission track lengths and crystallographic orientation were measured using a digitizing tablet interfaced with a computer at 2000x magnification under unpolarized light. Only natural, horizontal, confined fission tracks with clearly visible ends were measured. The mean D_{par} was determined for each grain by measuring up to four etch pit diameters. Fission track grain ages were calculated using a modified form of the radioactive decay equation and the ratio of the number of fission tracks present to the concentration of ^{238}U measured using laser ablation-inductively coupled plasma-mass spectrometry (LA-ICP-MS) [*Donelick et al.*, 2005; *Hasebe et al.*, 2004]. This decay equation includes a zeta calibration factor, which was determined by analyzing Durango and Fish Canyon apatite (30.6 ± 0.3 Ma from Cerro de Mercado, Durango, Mexico and 27.9 ± 0.7 Ma from the San Juan Mountains, Colorado, USA) at the beginning and end of each LA-ICP-MS session for its U:Ca ratio.

Appendix B: Thermal Modeling

We performed inverse thermal modeling of our AFT data using the software HeFTy version 1.7.4 [Ketcham et al. 2005]. We used the multi-kinetic annealing model of Ketcham et al. [1999] and included D_{par} values. We projected the track lengths to the crystallographic c-axis [Donelick et al. 1999] and included ^{252}Cf irradiation.

We began with an initial, open-ended model open-ended model was performed with all sample data as one kinetic population with a starting temperature of (1) 200°C at a time that is 50 Ma older than deposition and (2) 20°C at present (after Barnes et al. [2006; 2008]). We ran this model to assess how distinct the recent cooling history is without bias from user-defined constraints. We then simulated source region exhumation and subsequent incorporation of apatite grains into sedimentary bedrock samples by forcing the time-temperature paths to travel from depth (200°C) 50 Myr before sample deposition to surficial conditions (10-30°C) during deposition, then to reheat (50-180°C) between deposition and 1 Ma before returning to the surface (20°C) by the present. By comparing the two models, we could confirm that the refined model better constrains the same cooling event as the open-ended model, ensuring that we imposed realistic modeling parameters that did not remove the intrinsic cooling history. We designated each time-temperature cooling path segment to be monotonic for simplicity. For maximum flexibility [see *Ketcham*, 2005] thermal history segments between each imposed t-T constraints were designated as episodic style, random spacing, with the largest number of vertices (halved 5 times). We enforced a maximum slope of 40ºC/Myr, assuming that cooling rates on the FTB structures will be similar to or lower than in the

Axial Zone [e.g. *Metcalf*, 2009]. We ran each inversion with a Monte Carlo search and 50,000 attempted paths.

Appendix C: RadialPlotter Results

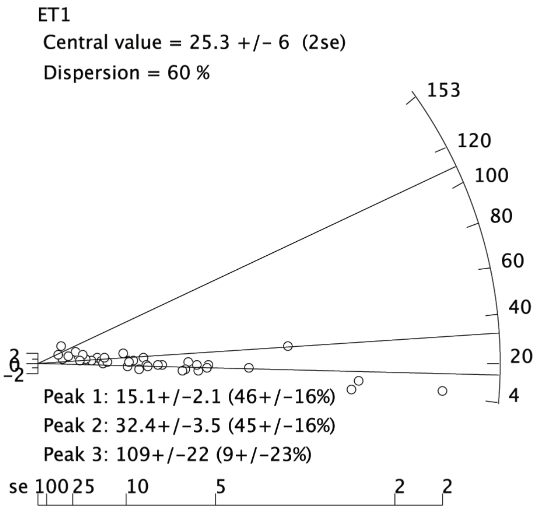

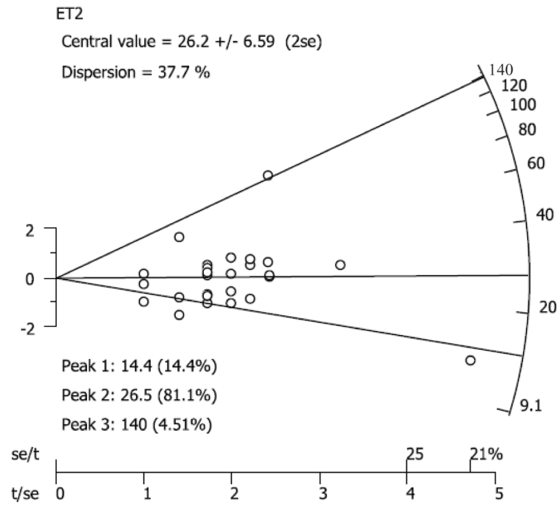

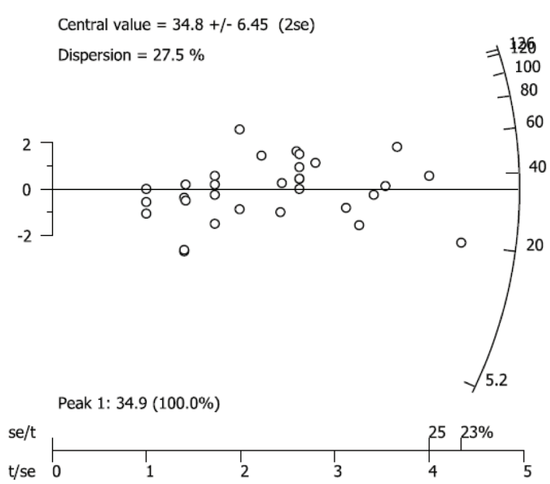

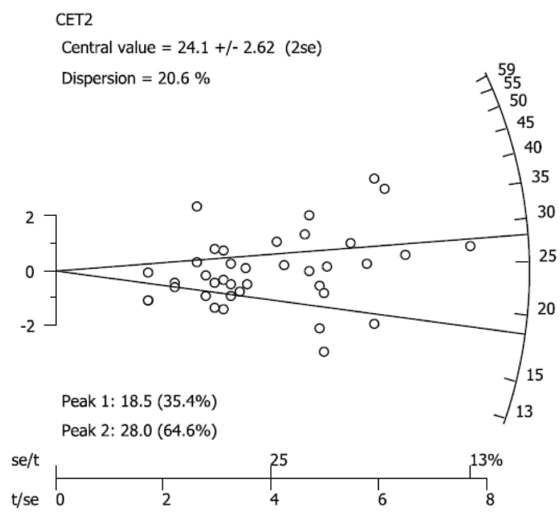

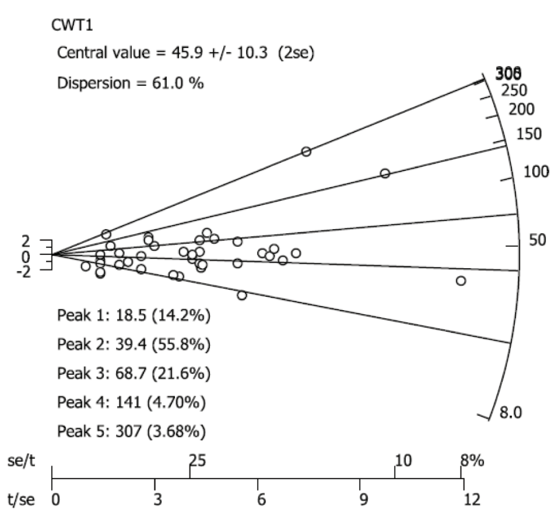

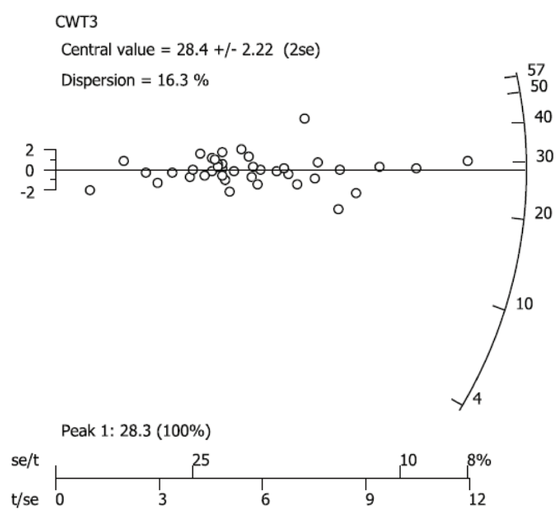

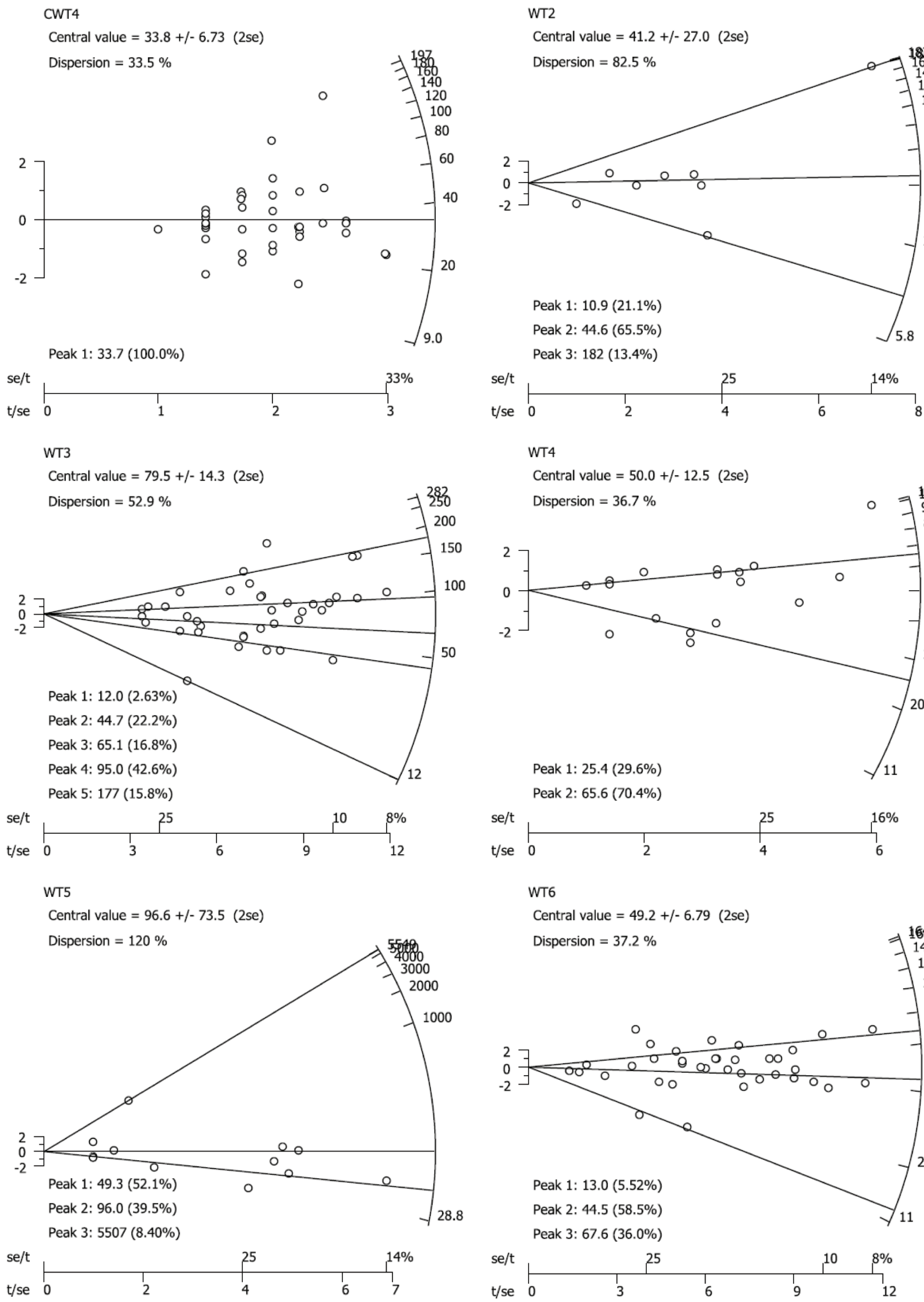
CWT4
Central value = 33.8 +/- 6.73 (2se)
Dispersion = 33.5 %
Peak 1: 33.7 (100.0%)
WT2
Central value = 41.2 +/- 27.0 (2se)
Dispersion = 82.5 %
Peak 1: 10.9 (21.1%)
Peak 2: 44.6 (65.5%)
Peak 3: 182 (13.4%)
WT3
Central value = 79.5 +/- 14.3 (2se)
Dispersion = 52.9 %
Peak 1: 12.0 (2.63%)
Peak 2: 44.7 (22.2%)
Peak 3: 65.1 (16.8%)
Peak 4: 95.0 (42.6%)
Peak 5: 177 (15.8%)
WT4
Central value = 50.0 +/- 12.5 (2se)
Dispersion = 36.7 %
Peak 1: 25.4 (29.6%)
Peak 2: 65.6 (70.4%)
WT5
Central value = 96.6 +/- 73.5 (2se)
Dispersion = 120 %
Peak 1: 49.3 (52.1%)
Peak 2: 96.0 (39.5%)
Peak 3: 5507 (8.40%)
WT6
Central value = 49.2 +/- 6.79 (2se)
Dispersion = 37.2 %
Peak 1: 13.0 (5.52%)
Peak 2: 44.5 (58.5%)
Peak 3: 67.6 (36.0%)
se/t
t/se

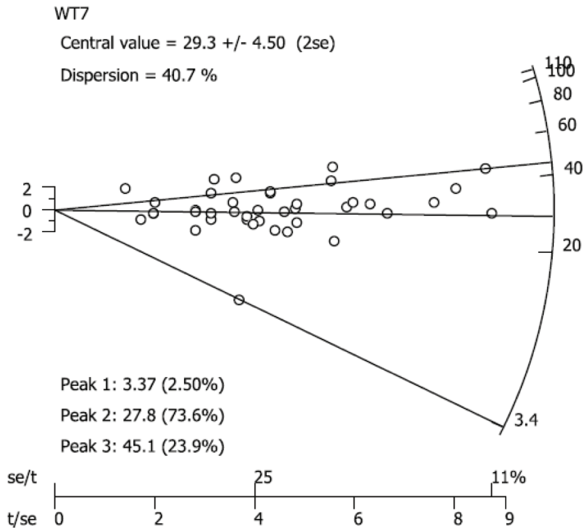
WT7
Central value = 29.3 +/- 4.50 (2se)
Dispersion = 40.7 %
Peak 1: 3.37 (2.50%)
Peak 2: 27.8 (73.6%)
Peak 3: 45.1 (23.9%)
se/t
t/se
110
100
80
60
40
20
3.4
25
11%

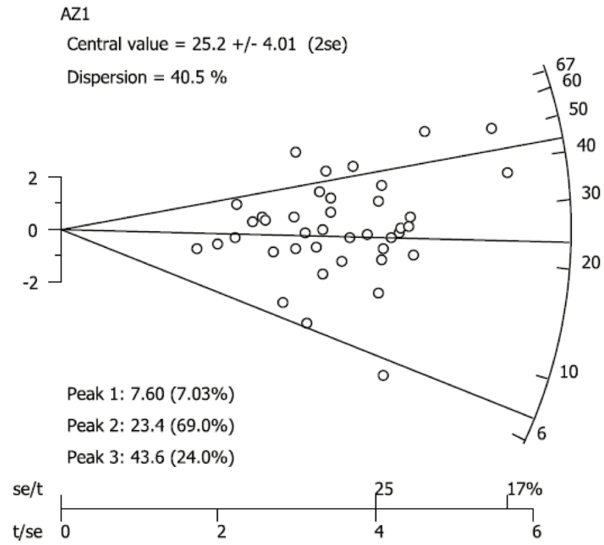
AZ1
Central value = 25.2 +/- 4.01 (2se)
Dispersion = 40.5 %
Peak 1: 7.60 (7.03%)
Peak 2: 23.4 (69.0%)
Peak 3: 43.6 (24.0%)
se/t
t/se
67
60
50
40
30
20
10
6
25
17%

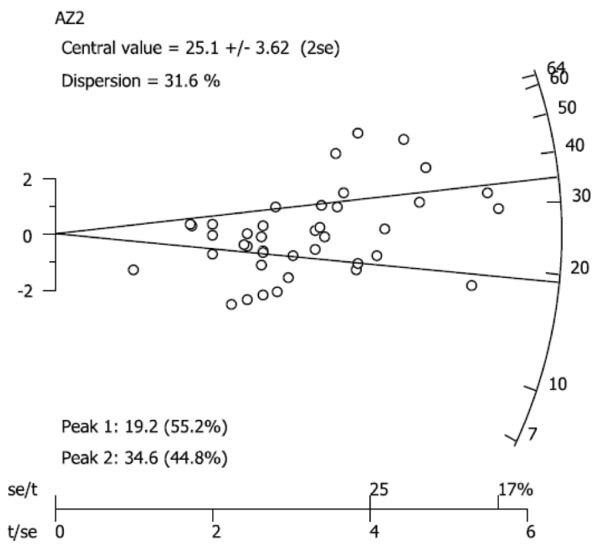
AZ2
Central value = 25.1 +/- 3.62 (2se)
Dispersion = 31.6 %
Peak 1: 19.2 (55.2%)
Peak 2: 34.6 (44.8%)
se/t
t/se
64
60
50
40
30
20
10
7
25
17%

REFERENCES

Allen, Philip A. (2008), From landscapes into geological history, *Nature*, *451*, 274-276

Arche, A., Evans, G., and E. Clavell (2010), Some considerations on the initiation of the present SE Ebro river drainage system: Post- or pre-Messinian? *Journal of Iberian Geology, 36*(1) 73-85

Ardevol, L., J. Klimowitz, J. Malagon, and P. J. C. Nagtegaal (2000), Depositional sequence response to foreland deformation in the Upper Cretaceous of the southern Pyrenees, Spain, *AAPG Bulletin*, *84*(4), 566-587

Argand, E. (1916), Sur l'arc des Alpes occidentales, *Eclogae Geologicae Hevetiae*, *14*, 145-191

Barnes, J. B., T. A. Ehlers, N. McQuarrie, P. B. O'Sullivan, and J. D. Pelletier (2006), Eocene to recent variations in erosion across the central Andean fold-thrust belt, northern Bolivia: Implications for plateau evolution, *Earth and Planetary Science Letters*, *248*, 118-133

Barnes, J. B., T. A. Ehlers, N. McQuarrie, P. B. O'Sullivan, and S. Tawackoli (2008), Thermochronometer record of central Andean Plateau growth, Bolivia (19.5 S), *Tectonics*, *27*, doi: 10.1029/2007TC002174

Beamud, E., J. A. Muñoz, P. G. Fitzgerald, S. L. Baldwin, M. Garcés, L. Cabrera, and J. R. Metcalf (2010), Magnetostratigraphy and detrital apatite fission track thermochronology in syntectonic conglomerates: constraints on the exhumation of the South-Central Pyrenees, *Basin Research*, doi: 10.1111/j.1365-2117.2010.00492.x

Beaumont, C., P. Fullsack, and J. Hamilton (Eds.) (1992), *Erosional control of active compressional orogens*, 18 pp., Chapman and Hall, London.

Beaumont, C., J. A. Muñoz, J. Hamilton, and P. Fullsack (2000), Factors controlling the Alpine evolution of the central Pyrenees inferred from a comparison of observations and geodynamical models, *Journal of Geophysical Research*, *105*, 8121-8145

Bollinger, L., P. Henry, and J. P. Avouac (2006), Mountain building in the Nepal Himalaya: Thermal and kinematic model, *Earth and Planetary Science Letters*, *244*, 58-71

Brandon, M. T., and J. A. Vance (1992), Tectonic evolution of the Cenozoic Olympic Subduction Complex, Washington State, as deduced from fission track ages for detrital zircons, *American Journal of Science*, *292*, 565-636

Brandon, M. T., M. K. Roden-Tice, and J. I. Garver (1998), Late Cenozoic exhumation of the Cascadia accretionary wedge in the Olympic Mountains, northwest Washington State, *Geological Society of America Bulletin*, *110*(8), 985-1009

Burbank, D. W., C. Puigdefàbregas, and J. A. Muñoz (1992b), The chronology of the Eocene tectonic and stratigraphic development of the eastern Pyrenean foreland basin, northeast Spain, *Geological Society of America Bulletin*, *104*, 1101-1120

Burbank, D. W., J. Vergés, J. A. Muñoz, and P. Bentham (1992a), Coeval hindward- and forward-imbricating thrusting in the south-central Pyrenees, Spain: Timing and rates of shortening and deposition, *Geological Society of America Bulletin*, *104*, 3-17

Burtner, R. L., A. Nigrini, and R. A. Donelick (1994), Thermochronology of Lower Cretaceous source rocks in the Idaho-Wyoming thrust belt, *American Association of Petroleum Geologists Bulletin*, *78*(10), 1613-1636

Cabrera, L., M. Cabrera, R. Gorchs, and F. X. C. de las Heras (2002), Lacustrine basin dynamics and organosulphur compound origin in a carbonate-rich lacustrine system (Late Oligocene Mequinenza Formation, SE Ebro Basin, NE Spain), *Sedimentary Geology*, *148*, 289-317

Capote, R., J. A. Muñoz, J. L. Simon, C. L. Liesa, and l. E. Arlegui (2002), Alpine tectonics I: the Alpine system north of the Betic Cordillera, in *The Geology of Spain*, edited by W. Gibbons and T. Moreno, pp. 367-400, The Geological Society Publishing House, Bath, UK.

Carlson, W. D., R. A. Donelick, and R. A. Ketcham (1999), Variability of apatite fission-track annealing kinetics: I. Experimental results, *American Mineralogist*, *84*, 1213-1223
Catalunya, I. C. d. (2003), Mapa geologic de Catalunya 1:250,000, Barcelona.

Chapple, W. M. (1978), Mechanics of thin-skinned fold-and-thrust belts, *Geological Society of America Bulletin*, *89*, 1189-1198

Coney, P. J., J. A. Muñoz, K. R. McClay, and C. A. Evenchick (1996), Syntectonic burial and post-tectonic exhumation of the southern Pyrenees foreland fold-thrust belt, *Journal of the Geological Society, London*, *153*, 9-16

Costa, E., M. Garcés, M. López-Blanco, E. Beamud, M. Gomez-Paccard, and J. C. Larrasoana (2009), Closing and continentalization of the South Pyrenean foreland basin (NE Spain): magnetochronological constraints, *Basin Research*, doi: 10.1111/j.1365-2117.2009.00452.x

Dahlen, F. A., J. Suppe, and D. Davis (1984), Mechanics of Fold-and-Thrust Belts and Accretionary Wedges: Cohesive Coulomb Theory, *Journal of Geophysical Research*, *89*(B12), 10,087-010,101

Davis, D., J. Suppe, and F. A. Dahlen (1983), Mechanics of fold-and-thrust belts and accretionary wedges, *Journal of Geophysical Research*, *88*(B2), 1153-1172

DeCelles, P. G., and G. Mitra (1995), History of the Sevier orogenic wedge in terms of critical taper models, northeast Utah and southwest Wyoming, *Geological Society of America Bulletin*, *107*(4), 454-462

DeCelles, P. G., and K. A. Giles (1996), Foreland basin systems, *Basin Research*, *8*, 105-123

Dodson, M. H. (1973), Closure temperature in cooling geochronological and petrological systems, *Contributions to Mineralogy and Petrology*, *40*, 259-274

Donelick, R. A., and D. S. Miller (1991), Enhanced tint fission track densities in low spontaneous track density apatites using 252Cf-derived fission fragment tracks: A model and experimental observations, *International Journal of Radiation Applications and Instrumentation. Part D. Nuclear Tracks and Radiation Measurements*, *18*(3), 301-307, doi: 10.1016/1359-0189(91)90022-a

Donelick, R. A., P. B. O'Sullivan, and R. A. Ketcham (2005), Apatite fission-track analysis, *Reviews in Mineralogy and Geochemistry*, *58*, 49-94

Ehlers, T. A. (2005), Crustal thermal processes and the interpretation of thermochronometer data, *Reviews in Mineralogy and Geochemistry*, *58*, 315-350

Filleaudeau, P.-Y., F. Mouthereau, and R. Pik (2011), Thermo-tectonic evolution of the south-central Pyrenees from rifting to orogeny: insights from detrital zircon U/Pb and (U-Th)/He thermochronometry, *Basin Research*, *23*, doi: 10.1111/j.1365-2117.2011.00535.x

Fillon, C., and P. van der Beek (2012), Post-orogenic evolution of the southern Pyrenees: constraints from inverse thermo-kinematic modelling of low-temperature thermochronology data, *Basin Research*, *23*, doi: 10.1111/j.1365-2117.2011.00533.x

Fillon, C., P. van der Beek, and C. Gautheron (2010), Post-orogenic evolution of the Southern Pyrenees: Thermokinematic modeling and (U-Th)/He dating, in *Thermo2010 12th International Conference on Thermochronology*, edited, p. 306, Glasgow, Scotland.

Fitzgerald, P. G., J. A. Muñoz, P. J. Coney, and S. L. Baldwin (1999), Asymmetric exhumation across the Pyrenean orogen: implications for the tectonic evolution of a collisional orogen, *Earth and Planetary Science Letters*, *173*, 157-170

Fleischer, R. L., P. B. Price, and R. M. Walker (1975), *Nuclear Tracks in Solids*, University of California Press, Berkeley and Los Angelos.

Galbraith, R. F. (1981), On statistical models for fission track counts, *J. Int. Assoc. Math.Geol.*, *13*, 471-478

Galbraith, R. F., and P. F. Green (1990), Estimating the component ages in a finite mixture, *Nuclear Tracks and Radiation Measurements*, *17*, 197-206

Gallagher, K., R. Brown, and C. Johnson (1998), Fission track analysis and its applications to geological problems, *Annual Reviews in Earth and Planetary Sciences*, *26*, 519-572

Garcia-Castellanos, D., J. Vergés, J. Gaspar-Escribano, and S. Cloetingth (2003), Interplay between tectonics, climate, and fluvial transport during the Cenozoic evolution of the Ebro Basin (NE Iberia), *Journal of Geophysical Research*, *108*

Gibson, M., H. D. Sinclair, G. J. Lynn, and F. M. Stuart (2007), Late- to post-orogenic exhumation of the Central Pyrenees reveal through combined thermochronological data and modelling, *Basin Research*, *19*, 323-334

Gleadow, A. J. W., I. R. Duddy, P. F. Green, and J. F. Lovering (1986), Confined fission track lengths in apatite: a diagnostic tool for thermal history analysis, *Contributions to Mineralogy and Petrology*, *94*, 405-415

Green, P. F. (1981), A new look at statistics in fission-track dating, *Nuclear Tracks and Radiation Measurements*, *5*, 77-86

Gunnell, Y., M. Calvet, S. Brichau, A. Carter, J. P. Aguilar, and H. Zeyen (2009), Low long-term erosion rates in high-energy mountian belts: Insights from thermo- and biochronology in the Eastern Pyrenees, *Earth and Planetary Science Letters*, *278*, 208-218

Haines, S. H. (2008), Transformations in clay-rich fault rocks: Constraining fault zone processes and the kinematic evolution of regions, 42 pp, University of Michigan, Ann Arbor.

Hamer, J. M. M., N. D. Sheldon, and G. J. Nichols (2007), Global aridity during the early Miocene? A terrestrial paleoclimate record from the Ebro Basin, Spain, *Journal of Geology*, *114*, 601-608

Hasebe, N., J. Barbarand, K. Jarvis, A. Carter, and A. J. Hurford (2004), Apatite fission-track chronometry using laser ablation ICP-MS, *Chemical Geology*, *207*(3-4), 135-145, doi: 10.1016/j.chemgeo.2004.01.007

Hogan, P. J., and D. W. Burbank (1996), Evolution of the Jaca piggyback basin and emergence of the External Sierra, southern Pyrenees, in *Tertiary Basins of Spain*, edited by P. F. Friend and C. J. Dabrio, pp. 153-160, Cambridge University Press.

Jolivet, M., P. Labaume, P. Monie, M. Brunel, N. Arnaud, and M. Campani (2007), Thermochronology constraints for the propogation sequence of the south Pyrenean basement thrust system (France-Spain), *Tectonics*, *26*, doi: 10.1029/2006TC002080

Ketcham, R. A. (2005), Forward and inverse modeling of low-temperature thermochronometry data, *Reviews in Mineralogy and Geochemistry*, *58*, 275-314

Ketcham, R. A., R. A. Donelick, and W. D. Carlson (1999), Variability of apatite fission-track annealing kinetics: III. Extrapolation to geological time scales, *American Mineralogist*, *84*, 1235-1255

Lewis, C. J., J. Vergés, and M. Marzo (2000), High mountains in a zone of extended crust: Insights into the Neogene-Quaternary topographic development of northeastern Iberia, *Tectonics*, *19*, 86-102

McQuarrie, N., and P. G. DeCelles (2001), Geometry and structural evolution of the central Andean backthrust belt, Bolivia, *Tectonics*, *20*(5), doi: 10.1029/2000TC001232

McQuarrie, N., T. A. Ehlers, J. B. Barnes, and B. Meade (2008), Temporal variation in climate and tectonic coupling in the central Andes, *Geology*, *36*(12), 999-1002, doi: 10.1130/G25124A.1

Meigs, A. J., and D. W. Burbank (1997), Growth of the south Pyrenean orogenic wedge, *Tectonics*, *16*(2), 239-258

Meigs, A. J., J. Vergés, and D. W. Burbank (1996), Ten-million-year history of a thrust sheet, *Geological Society of America Bulletin*, *108*(12), 1608-1625

Metcalf, J. R., Paul G. Fitzgerald, Suzanne L. Baldwin, Josep-Anton Muñoz (2009), Thermochronology of a convergent orogen: Constraints on the timing of thrust faulting and subsequent exhumation of the Maladeta Pluton in the Central Pyrenean Axial Zone, *Earth and Planetary Science Letters*, *287*, 488-503

Mitra, G., and A. J. Sussman (1997), Structural evolution of connecting splay duplexes and their implications for critical taper: an example based on geometry and kinematics of the Canyon Range culmination, Sevier Belt, central Utah, *Journal of Structural Geology*, *19*(3-4), 503-521

Mitra, G., K. Bhattacharyya, and M. Mukul (2010), The Lesser Himalayan Duplex in Sikkim: Implications for variations in Himalayan shortening, *Journal Geological Society of India*, *75*(289-301)

Morris, R. G., H. D. Sinclair, and A. J. Yelland (1998), Exhumation of the Pyrenean orogen: implications for sediment discharge, *Basin Research*, *10*, 69-85

Mugnier, J. L., P. Baby, B. Colletta, P. Vinour, P. Bale, and Leturmy (1997), Thrust geometry controlled by erosion and sedimentation: a view from analogue models, *Geology*, *25*(5), 427-430

Muñoz, J. A. (1992), Evolution of a continental collision belt: ECORS-Pyrenees crustal balanced cross-section, *Thrust Tectonics*

Rahl, J. M., S. H. Haines, and B. A. van der Pluijm (2011), Links between orogenic wedge deformation and erosional exhumation: Evidence from illite age analysis of fault rock and detrital thermochronology of syn-tectonic conglomerates in the Spanish Pyrenees, *Earth and Planetary Science Letters*, *307*, 180-190

Ramos, E., P. Busquets, and J. Vergés (2002), Interplay between longitudinal fluvial and transverse alluvial fan systems and growing thrusts in a piggyback basin (SE Pyrenees), *Sedimentary Geology*, *146*, 105-131

Reiners, P. W., and M. T. Brandon (2006), Using thermochronology to understand orogenic erosion, *Annual Reviews in Earth and Planetary Sciences*, *34*, 419-466

Sibuet, J.-C., S. P. Srivastava, and W. Spakman (2004), Pyrenean orogeny and plate kinematics, *Journal of Geophysical Research*, *109*, doi: 10.1029/2003JB002514

Simpson, G. (2006), Influence of erosion and deposition on deformation in fold belts, *Geological Society of America Special Paper*, *398*, 67–281, doi: 10.1130/2006.2398(16)

Sinclair, H. D., M. Gibson, M. Naylor, and R. G. Morris (2005), Asymmetric growth of the Pyrenees revealed through measurement and modeling of orogenic fluxes, *American Journal of Science*, *305*, 369-406

Stockmal, G. S., C. Beaumont, M. Nguyen, and B. Lee (2007), Mechanics of thin-skinned fold-and-thrust belts: Insights from numerical models, in *Whence the Mountains? Inquiries into the Evolution of Orogenic Systems: A Volume in Honor of Raymond A. Price: Geological Society of America Special Paper* edited by J. W. Sears, T. A. Harms and C. A. Evenchick, pp. 63-98.

Storti, F., and K. R. McClay (1995), Influence of syntectonic sedimentation on thrust wedges in analogue models, *Geology*, *23*, 999-1002

Suppe, J. (1987), The Active Taiwan Mountain Belt, in *Anatomy of Mountain Chains*, edited by J. P. Schaer and J. Rodgers, pp. 277-293, Princeton University Press.

Tagami, T., and P. B. O'Sullivan (2005), Fundamentals of fission-track thermochronology, *Reviews in Mineralogy and Geochemistry*, *58*, 19-47

Teixell, A. (1998), Crustal structure and orogenic material budget in the west central Pyrenees, *Tectonics*, *17*(3), 395-406

Thiede, R. C., J. R. Arrowsmith, B. Bookhagen, M. O. McWilliams, E. R. Sobel, and M. R. Strecker (2005), From tectonically to erosionally controlled development of the Himalayan orogen, *Geology*, *33*(8), 689-692

Vergés, J. (1999), Estudi geologic del vessant sud del Pirineu oriental i central. Evolucio cinematica en 3D., *Servei Geologic, Monografia Tecnica*, *7*, 192 pp.

Vergés, J., and J. A. Muñoz (1990), Thrust sequences in the southern central Pyrenees, *Bulletin de la Societe Geologique de France*, *8*, 265-271

Vergés, J., and D. W. Burbank (Eds.) (1996), *Eocene-Oligocene thrusting and basin configuration in the eastern and central Pyrenees (Spain)*, Cambridge University press.

Vergés, J., M. Fernàndez, and A. Martínez (2002), The Pyrenean orogen: pre-, syn-, and post-collisional evolution, *Journal of the Virtual Explorer*, *8*, 55-74

Vergés, J., H. Millán, E. Roca, J. A. Muñoz, M. Marzo, J. Cires, T. D. Bezemer, R. Zoetemeijer, and S. Cloetingth (1995), Eastern Pyrenees and related foreland basins: pre-, syn-, and post-collisional crustal-scale cross-sections, *Marine and Petroleum Geology*, *12*(8), 893-915

Vermeesch, P. (2008), RadialPlotter: a Java application for fission track, luminescence and other radial plots, *Radiation Measurements*, *44*(4), 409-410

Whitchurch, A. L., A. Carter, H. D. Sinclair, R. A. Duller, A. C. Whittaker, and P. A. Allen (2011), Sediment routing system evolution within a diachronously uplifting orogen: insights from detrital zircon thermochronological analyses from the south-central Pyrenees, *American Journal of Science*, *311*, 442-482

Willett, S. D. (1999), Orogeny and orography: the effects of erosion on the structure of mountain belts, *Journal of Geophysical Research*, *104*(B12), 28,957-28981

Willett, S. D., C. Beaumont, and P. Fullsack (1993), Mechanical model for the tectonics of doubly vergent compressional orogens, *Geology*, *21*, 371-374

Zachos, J. C., M. Pagani, L. Sloan, E. Thomas, and K. Billups (2001), Trends, rhythms, and aberrations in global climate 65 Ma to present, *Science*, *292*, 686-693